JOURNAL OF GEOPHYSICAL RESEARCH, VOL. 106, NO. D19, PAGES 22,931–22,964, OCTOBER 16, 2001

Effects of aerosols on tropospheric oxidants: A global model study

Xuexi Tie, Guy Brasseur,[1] and Louisa Emmons

National Center for Atmospheric Research, Boulder, Colorado, USA

Larry Horowitz

Geophysical Fluid Dynamics Laboratory, Princeton University, Princeton, New Jersey, USA

Douglas Kinnison

National Center for Atmospheric Research, Boulder, Colorado, USA

Abstract. The global distributions of sulfate and soot particles in the atmosphere are calculated, and the effect of aerosol particles on tropospheric oxidants is studied using a global chemical/transport/ aerosol model. The model is developed in the framework of the National Center for Atmospheric Research (NCAR) global three-dimensional chemical/transport model (Model for Ozone and Related Chemical Tracers (MOZART)). In addition to the gas-phase photochemistry implemented in the MOZART model, the present study also accounts for the formation of sulfate and black carbon aerosols as well as for heterogeneous reactions on particles. The simulated global sulfate aerosol distributions and seasonal variation are compared with observations. The seasonal variation of sulfate aerosols is in agreement with measurements, except in the Arctic region. The calculated vertical profiles of sulfate aerosol agree well with the observations over North America. In the case of black carbon the calculated surface distribution is in fair agreement with observations. The effects of aerosol formation and heterogeneous reactions on the surface of sulfate aerosols are studied. The model calculations show the following: (1) The concentration of H_2O_2 is reduced when sulfate aerosols are formed due to the reaction of SO_2 + H_2O_2 in cloud droplets. The gas-phase reaction SO_2 + OH converts OH to HO_2, but the reduction of OH and enhancement of HO_2 are insignificant (< 3%). (2) The heterogeneous reaction of HO_2 on the surface of sulfate aerosols produces up to 10% reduction of hydroperoxyl radical (HO_2) with an uptake coefficient of 0.2. However, this uptake coefficient could be overestimated, and the results should be regard as an upper limit estimation. (3) The N_2O_5 reaction on the surface of sulfate aerosols leads to an 80% reduction of NO_x at middle to high latitudes during winter. Because ozone production efficiency is low in winter, ozone decreases by only 10% as a result of this reaction. However, during summer the N_2O_5 reaction reduces NO_x by 15% and O_3 by 8-10% at middle to high latitudes. (4) The heterogeneous reaction of CH_2O on sulfate aerosols with an upper limit uptake coefficient ($\gamma = 0.01$) leads to an 80 to 90% decrease in CH_2O and 8 to 10% reduction of HO_2 at middle to high latitudes during winter. Many uncertainties remain in our understanding of heterogeneous chemical processes and in the estimate of kinetic parameters. This model study should therefore be regarded as exploratory and subject to further improvements before final conclusions can be made.

1. Introduction

Tropospheric aerosols are suspended particles, including condensed water, sulfate droplets, sea-salt particles, black carbon/soot, silicates, and organic aerosols. There has been increased recognition of the importance of aerosols in climate change and climate prediction. Aerosols affect the climate both directly, through scattering and absorption of incoming solar radiation, and indirectly, through their ability to act as cloud condensation nuclei (CCN). Studies [*Charlson et al.*, 1991; *Kiehl and Briegleb*, 1993; *Penner et al.*, 1994] suggest that the globally averaged effects of aerosols may be similar in magnitude but opposite in sign to the projected warming attributed to greenhouse gas accumulation. Because aerosols are far from being uniformly distributed in the atmosphere, their radiative forcing varies considerably in space and can exceed substantially the effect of well-mixed greenhouse gases in regions of intense biomass burning and fossil fuel consumption.

Aerosol particles also have strong interactions with oxidants in the atmosphere. Multiphase and heterogeneous reactions on and

[1]Now at Max-Planck-Institute of Meteorology, Hamburg, Germany.

Paper number 2001JD900206.
0148-0227/01/2001JD900206$09.00

within aerosols have the potential to play a major role in determining the composition of the gaseous atmosphere. The interaction between aerosols and gas composition is a relatively new research area. The studies of the effects of Polar Stratospheric Clouds (PSCs) and sulfate aerosols on chemical composition in the lower stratosphere have shown that heterogeneous reactions on the surface of these particles play an important role in determining ozone concentrations in the stratosphere [*Solomon et al.*, 1986; *Hofmann and Solomon*, 1989; *Brasseur et al.*, 1990; *Pitari and Rizi*, 1993; *Hofmann et al.*, 1994; *Tie et al.*, 1996]. However, it is only recently that the effects of aerosols on tropospheric chemistry have been stressed [see, e.g., *Lelieveld and Crutzen*, 1990; *Dentener and Crutzen*, 1993; *Kolb et al.*, 1995; *Dentener and Crutzen*, 1996; *Hauglustaine et al.*, 1996; *Andreae and Crutzen*, 1997; *Ravishankara,* 1997; *Saylor,* 1997; *Aumont*, 1999; *Jacob*, 2000; *Thomas et al.*, 2001], and many uncertainties remain and will need to be addressed in the future.

In this paper, we develop a coupled chemical/aerosol model to address the interaction between sulfate and black carbon aerosols and tropospheric composition. Several global sulfate and black carbon aerosol models have been developed in the past [*Benkovitz et al.*, 1996; *Chin et al.*, 1996; *Cooke and Wilson*, 1996; *Feichter et al.*, 1996; *Liousse et al.*, 1996; *Kasibhatla et al.*, 1997; *Barth et al.*, 2000] in an off-line mode, with gas-phase chemical species concentrations provided as input data and the impact of aerosol particles on gas-phase compounds ignored. In this paper, we will present an interactive model which has several advantages: (1) The formation of sulfate aerosol particles depends strongly upon the diurnal variations of radical OH and NO_3, which are generally not simulated by off-line models; (2) the perturbations of gas-phase species resulting from the formation of aerosols are fully accounted for; (3) the feedbacks on the aerosol formation from changing concentrations of gas-phase compounds (resulting from heterogeneous reactions) are taken into account.

This study is not intended to be comprehensive and account for all processes affecting aerosol/gas-phase interactions. For example, suggested by *Dentener et al.* [1996], the reaction of SO_2 on calcium-rich mineral dust is likely to play an important role. The interactions of N_2O_5, O_3, and HO_2 with mineral dust are affecting to affect the photochemical oxidants, causing ozone decreases of perhaps 10% in and nearby the dust source areas. However, mineral dust is not included in the present version of the MOZART model, and the heterogeneous reactions on mineral dust will not be discussed in the present study. Furthermore, the model does not account for the impact of aerosol radiative effects on the photochemistry. For example, the presence of aerosols affect the photolysis rate of chemical species [*He and Carmichael*, 1999; *Liao et al.*, 1999]. This process, which could lead to changes in the concentration of tropospheric oxidants, is not considered in the present study.

The paper is divided into several sections. Section 2 provides a brief description of the chemical/aerosol/transport model that will be used in the study, Section 3 shows the simulation of particle distributions and comparison with observations, and Section 4 discusses the effects of heterogeneous reactions on the tropospheric composition.

2. Description of the Model

The model providing the mass density of sulfate and black carbon particles is developed in the framework of the National Center for Atmospheric Research (NCAR) global three-dimensional chemical/transport model (Model for Ozone and Related Chemical Tracers (MOZART), version 1). MOZART 1 [*Brasseur et al.*, 1998] is a comprehensive tropospheric chemical/transport model, calculating the global distribution of 56 gas-phase chemical species (see Table 1 of *Brasseur et al.* [1998]). In the present study the concentrations of OH, H_2O_2, NO_3, and O_3 are used to calculate the conversion of gas-phase sulfur species into sulfate aerosols. In addition, SO_2, $SO_4^=$, dimethyl sulfide (DMS), and NH3 are added to the gas-phase chemical scheme used in MOZART. The model is configured with a T42 (2.8° x 2.8°) horizontal resolution and 25 hybrid vertical levels ranging from the surface to 4 mbar. Meteorological information (i.e., winds, temperature, etc.) is provided by the NCAR Community Climate Model (CCM-2) every 3 hours based on precalculated results (off-line). The model time step for chemistry and transport is 20 minutes. Within a 3-hour period the meteorological variables are interpolated linearly with time. The chemical species are transported by advective [*Rasch and Williamson*, 1991], diffusive [*Holtslag and Boville*, 1993], and convective [*Hack et al.*, 1994] processes. Details on the treatment of gas-phase chemical mechanisms and transport processes are provided by *Brasseur et al.* [1998]. The distribution of CH4, nonmethane hydrocarbons (NMHCs), and CO calculated by MOZAR1 are generally consistent with observations [*Hauglustaine et al.*, 1998]. The seasonal cycle of ozone is generally well simulated in comparison with ozonesondes, although MOZART 1 tends to underestimate O_3 concentrations at middle and high latitudes of the Northern Hemisphere, especially in the upper troposphere due to the ozone flux across the tropopause being underestimated in the model. The nitric acid (HNO_3) mixing ratio and the HNO_3/NO_x concentration ratio are generally overestimated, especially over the Pacific Ocean and over North America.

2.1. Gas-Phase Sulfur and Sulfate Aerosols

The chemical scheme for gas-phase reactions implemented in MOZART 1 includes the oxidation of dimethyl sulfide (DMS) by OH and NO_3 as well as the conversion of SO_2 into sulfate by OH:

(R1) $DMS + OH \rightarrow SO_2 + products$,
(R2) $DMS + OH \rightarrow 0.75\ SO_2 + 0.25\ MSA$,
(R3) $DMS + NO_3 \rightarrow SO_2 + products$,
(R4) $SO_2 + OH \rightarrow SO_4^= + HO_2$.

The corresponding reaction coefficients are listed in Table 1. The reactions (R1)-(R4) do not represent single reactions, but a sequence of reactions [*Chin et al.*, 1996]. Unlike previous model studies [*Benkovitz et al.*, 1994; *Chin et al.*, 1996; *Feichter et al.*, 1996; *Kasibhatla et al.*, 1997; *Barth et al.*, 2000], our approach allows for chemical feedbacks between sulfate and the oxidants included in the model. In the following sections, we show that the formation of sulfate aerosols can significantly affect OH concentrations in the polluted troposphere.

Aqueous phase conversion of SO_2 to $SO_4^=$ in cloud water is represented by the following reactions which become active in the grid cells of the model where clouds are present:

(R5) $SO_2(g) \Leftrightarrow SO_2(aq)$,
(R6) $O_3(g) \Leftrightarrow O_3(aq)$,
(R7) $H_2O_2(g) \Leftrightarrow H_2O_2(aq)$,
(R8) $SO_2(aq) \Leftrightarrow H^+ + HSO_3^-$,
(R9) $HSO_3^- \Leftrightarrow SO_3= + H^+$,
(R10) $S(IV) + H_2O_2(aq) \rightarrow SO_4^= + products$,
(R11) $S(IV) + O_3(aq) \rightarrow SO_4^= + products$,

Table 1. List of Gas-Phase Reactions, Gas-Aqueous Phase Equilibria, and Aqueous Phase Reaction Constants for Sulfate Aerosols[a]

Reactions	Coefficients	References
	Gas Phase	
1 $DMS + OH \rightarrow SO_2$ + products	$9.6x10^{-12}exp(-234/T)$	1
2 $DMS + OH \rightarrow 0.75\ SO_2 + 0.25$ MSA	a1/a2	1
	$a1=1.7x10^{-42}exp(7810/T)[O_2]$	
	$a2=1+5.5x10^{-31}exp(7460/T)[O_2]$	
3 $DMS + NO_3 \rightarrow SO_2$ + products	$1.9x10^{-13}exp(520/T)$	2
4 $SO_2 + OH \rightarrow H_2SO_4$	$[b1/(1+b1/b2)]\ 0.6^{b3}$	1
	$b1=3.0x10^{-31}x(300/T)^{3.3}[M]$	
	$b2=1.5x10^{-12}$	
	$b3=\{1+[log(b1/b2)]^2\}^{-1}$	
	Aqueous Phase	
5 $O_3(g) \leftrightarrow O_3(aq)$	$1.1x10^{-2}exp(2300(1/T-1/298))$	3
6 $H_2O_2(g) \leftrightarrow H_2O_2(aq)$	$7.4x10^{4}exp(6615(1/T-1/298))$	3
7 $H_2O(g) \leftrightarrow H^+ + OH^-$	$1.0x10^{-14}exp(-6716(1/T-1/298))$	3
8 $CO_2(g) \leftrightarrow CO_2(aq)$	$3.1x10^{-2}exp(2423.(1/T-1/298))$	3
9 $NH_3(g) \leftrightarrow NH_3(aq)$	$5.8x10^{1}exp(4085.(1/T-1/298))$	4
10 $SO_2(g) \leftrightarrow SO_2(aq)$	$1.23\ exp(3120.*(1/T-1/298))$	4
11 $HNO_3(g) \leftrightarrow HNO_3(aq)$	$2.1x10^{5}exp(8700(1/T-1/298))$	3
12 $NH_3(aq) \leftrightarrow NH_4^+ + OH^-$	$1.2x10^{-4}exp(-4325(1/T-1/298))$	4
13 $CO_2(aq) \leftrightarrow H^+ + HCO_3^-$	$4.3x10^{-7}exp(-913\ (1/T-1/298))$	4
14 $HNO_3(aq) \leftrightarrow H^+ + NO_3^-$	15.4	3
15 $SO_2(aq) \leftrightarrow H^+ + HSO_3^-$	$1.7x10^{-2}exp(2090)(1/T-1/298))$	4
16 $HSO_3^- \leftrightarrow H^+ + SO_3^=$	$6.0x10^{-8}exp(1120(1/T-1/298))$	4
17 $S(IV) = HSO_3^- + SO_3^=$		
18 $S(IV) + H_2O_2(aq) \rightarrow SO_4^=$ + products	$8x10^{4}exp(-3650(1/T-1/298))/c1$	5
	$c1=0.1+[H^+]$	
19 $S(IV) + O_3(aq) \rightarrow SO_4^=$ + products	$d1 + d2/[H^+]$	5
	$d1=4.39x10^{11}exp(-4131/T)$	
	$d2=2.56x0^{3}exp(-996/T)$	

[a]Here, 1, *Chin et al.* [1996]; 2, *Atkinson et al.* [1992]; 3, *Lelieveld* [1990]; 4, *Seinfeld* [1986]; 5, *Feichter et al.* [1996].

where (g) and (aq) correspond to gas and aqueous phase, respectively. S(IV) represents the sum of HSO_3^- and SO_3= ions dissolved in the aqueous phase. The rate constants and equilibrium constants for these reactions are listed in Table 1. As indicated in Table 1, the formation of sulfate in clouds depends strongly on the acidity of cloud droplets. Calculations by *Seinfeld* [1986] show that when water acidity is weak (pH > 5), the formation of $SO_4^=$ in the aqueous phase is dominated by (R7) whereas at low pH, sulfate is mainly formed by (R10). To explicitly calculate the formation of $SO_4^=$ in clouds, the acidity of the cloud water needs therefore to be calculated. We express the pH by

$$pH = -\log[H^+],$$

where $[H^+]$ represents the concentration of H^+ in the liquid phase with

$$[H^+] + [NH_4^+] = [OH^-] + [HCO_3^-] + [NO_3^-] + [HSO_3^-] + 2[SO_4^=].$$

Here $[OH^-]$ accounts for the dissociation of pure water, while $[HCO_3^-]$ results from the presence of dissolved carbon dioxide in the water droplets; $[NO_3^-]$ accounts for the effect of nitric acid, and $[NH_4^+]$ for the effect of ammonia on the overall acidity. *Dentener and Crutzen* [1994] have shown that ammonia is able to neutralize a great portion of the acids produced by the oxidation of sulfur and nitrogen oxides. The presence of ammonia, therefore, has an important impact on acids in clouds. Because the heterogeneous conversion of SO_2 to $SO_4^=$ depends strongly on cloud acidity (see Table 1), the presence of ammonia tends to enhance the formation of sulfate aerosols. Figure 1 shows the annually averaged surface ammonia concentrations. The highest concentrations are located in southern Asia, which is in agreement with the calculation of *Dentener and Crutzen* [1994]. The equilibrium constants for the dissolution and dissociation reactions are given in Table 1. The aqueous-phase reactions are solved separately from the gas- phase reactions.

Global emission inventories for SO_x (SO_2+$SO_4^=$) and DMS are taken from the International Global Atmospheric Chemistry/Global Emissions Inventory Activity (IGAC/GEIA) [*Benkovitz et al.*, 1994, 1996]. The original data, provided as monthly mean values at 1° x 1° horizontal resolution, have been interpolated to the 2.8° x 2.8° grid of the MOZART model. The emissions of SO_x are entirely anthropogenic with a global value of 67 Tg S/yr. Two percent of the total SO_x emissions are assumed to be in the form of $SO_4^=$. The global annually averaged emissions of SO_2 and DMS are shown in Plate 1. The SO_x emissions are very nonuniformly distributed, with the highest emissions located in the United States, Europe, and eastern Asia. The DMS emissions from the ocean provide a total of 15.5 Tg S/yr, and are highest in coastal areas. In the present study, the emissions of carbonyl sulfide (OCS), and the volcanic emission of SO_2 are not included

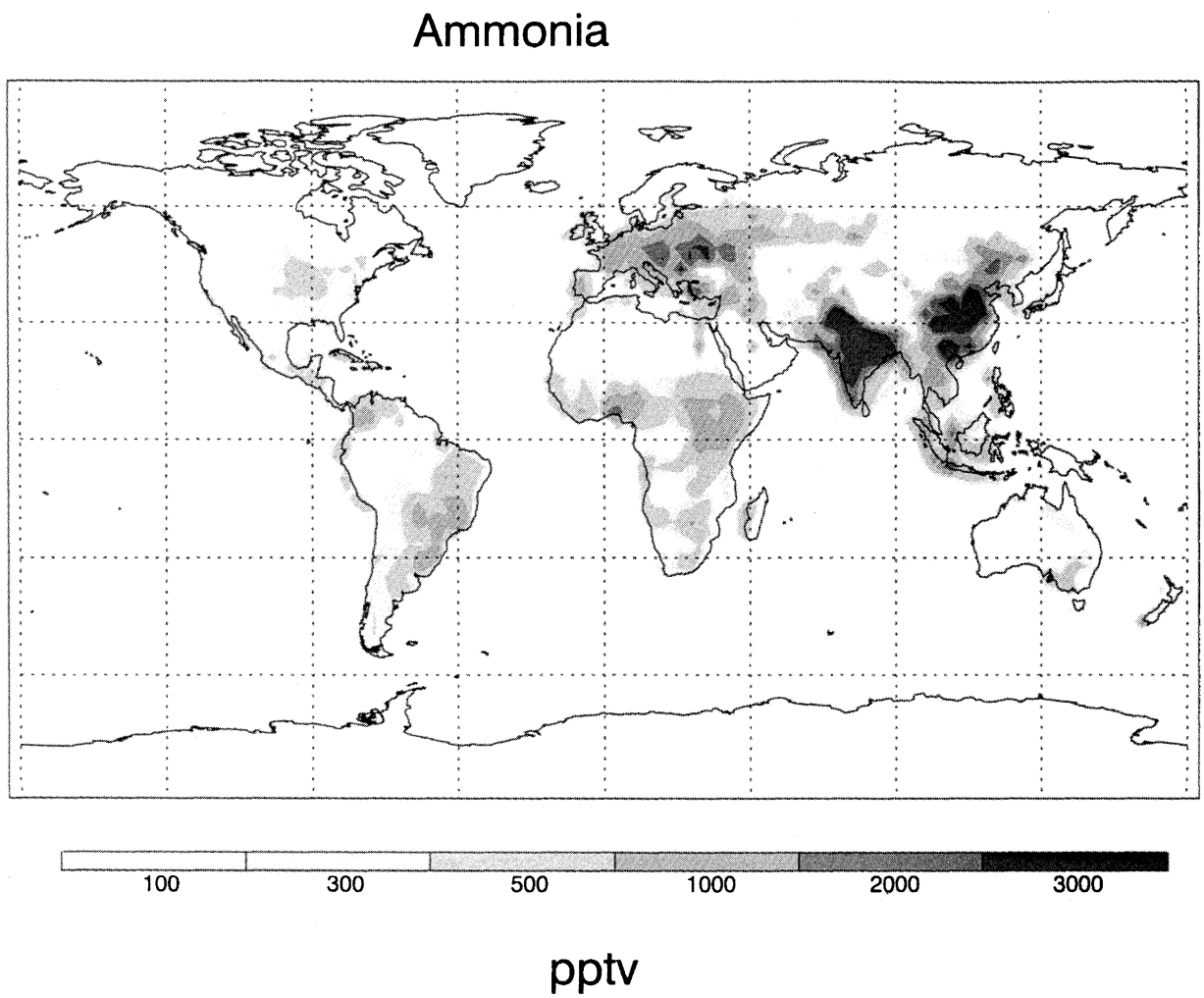

Figure 1. Calculated annually averaged surface concentrations (pptv) of ammonia.

in the model. These emissions strongly affect the formation of sulfate aerosols in the stratosphere [*Crutzen*, 1976; *Turco et al.*, 1979; *McCormick and Swissler*, 1983; *Visconti et al.*, 1988; *Tie et al.*, 1994a], but have small effects in the troposphere, especially in the boundary layer.

Removal of chemical compounds from the atmosphere is represented by dry deposition and wet scavenging. Dry deposition varies with surface characteristics and meteorological conditions near the surface [*Wesely and Hicks*, 2000]. In this model we use the simple parameterization suggested by *Feichter et al.* [1996], with a dry deposition velocity for SO_2 of 0.6 cm/s on the continents, 0.8 cm/s on the oceans, and 0.1 cm/s on snow. The dry deposition velocity for $SO_4^=$ [*Feichter et al.*, 1996] is assumed to be 0.2 cm/s on all surfaces. The dry deposition velocity of DMS is assumed to be zero. The wet deposition scheme includes in-cloud as well as below-cloud scavenging. The in-cloud scavenging is formulated according to the parameterization of *Giorgi and Chameides* [1985]. The rate of scavenging is a function of rainwater tendency and of the effective Henry's law constants. Very soluble species are also removed efficiently through below-cloud scavenging [*Levine and Schwartz*, 1982], using the formulation described by *Brasseur et al.* [1998]. For gas scavenging, the effective Henry's law constants are calculated according to the rate of uptake by raindrops, and the rate of dissociation inside the raindrop. According to the study of *Giorgi and Chameides* [1985], the scavenging rate for a gas with a low effective Henry law's constant is strongly dependent upon the solubility of this gas. However, for gases with high effective Henry's law constants (such as HNO_3 and H_2O_2), changes in solubility produce only very small changes in the rate of scavenging. In this case, the rate of wet scavenging is controlled primarily by the strength of rainfall. sulfate aerosols are assumed to be very soluble in raindrops [*Feichter et al.*, 1996], and their rate of scavenging is assumed to be the same as the rate of scavenging derived for HNO_3. The wet scavenging time constant for aerosol particles is of the order of a few days in the lower and middle troposphere (see *Brasseur et al.*, 1998), with a minimum scavenging time constant of 1 to 2 days in the tropics.

2.2. Black Carbon Particles

Black carbon is produced by the combustion of hydrocarbons [*Cooke and Wilson*, 1996; *Liousse et al.*, 1996]. Fossil fuel and biomass burning are therefore primary emissions of these particles. The global emissions of black carbon have been estimated by various authors to be 12 Tg C/yr [*Liousse et al.*, 1996], 18 Tg C/yr [*Cooke and Wilson*, 1996] to 24 Tg C/yr [*Penner et al.*, 1993]. The total emission used in this study is 12

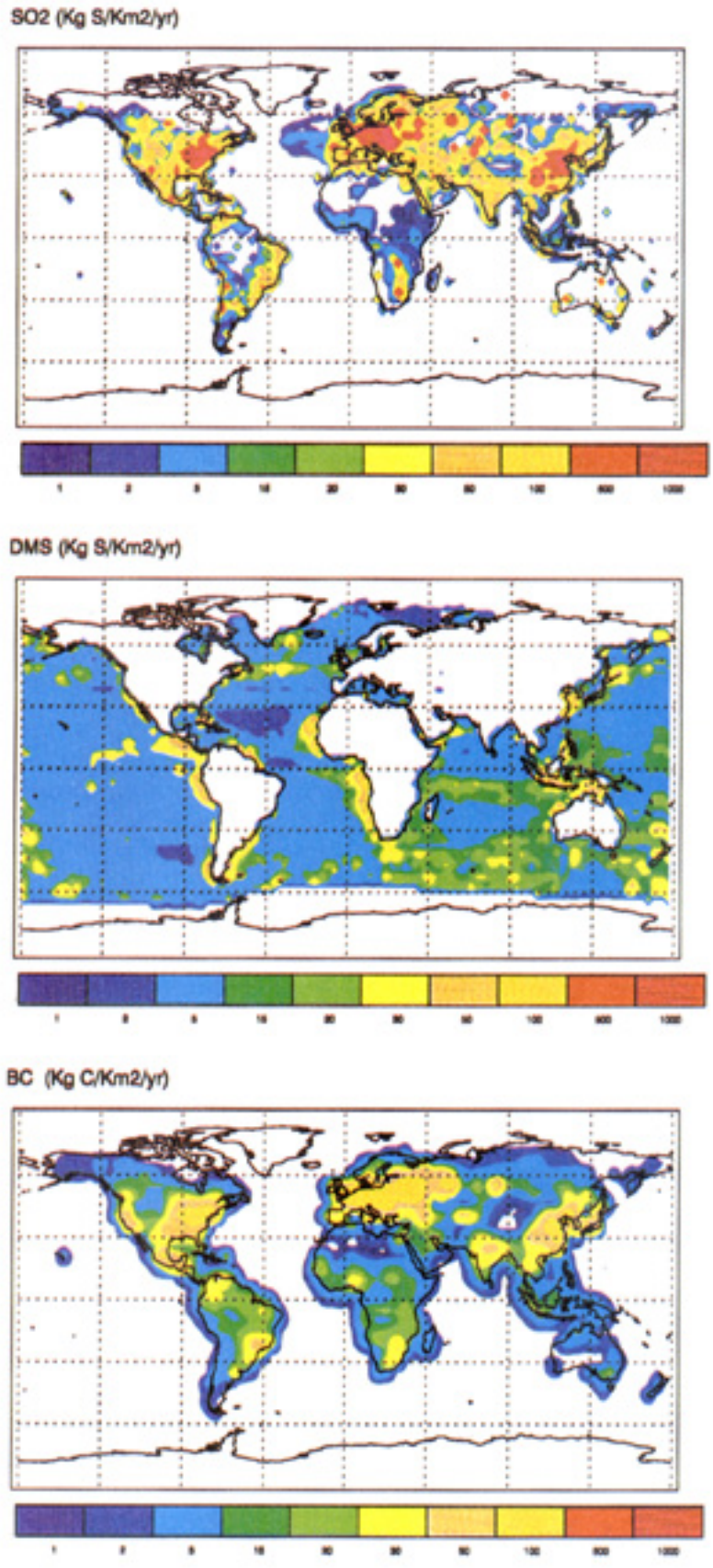

Plate 1. Annually averaged (top) SO_2, (middle) DMS, and (bottom) black carbon emissions (kg C km^{-2} y^{-1}) of the model.

Tg C/yr, which is on the low end of the previous studies, and is similar to the results recently suggested by *Liousse et al.* [1996]. *Ward et al.* [1996] and *Ferek et al.* [1998] suggest that black carbon emissions resulting from biomass burning are correlated with those of carbon monoxide (CO) produced by fires. In this study, we use the geographical and temporal distribution of CO emissions as implemented in the MOZART 1 model, with a black carbon emission scaled to 12 Tg C/yr. The annual average geographical distributions of black carbon emission are shown in Plate 1 (bottom panel). These emissions are large in Europe, eastern United States, and East Asia where large amounts of fossil fuel are burned. In Europe and in the eastern United States, emissions are highest. The contribution due to biomass burning is largest in the tropics, and its geographical distribution varies with season. Substantial black carbon emissions from large fires also occur in the boreal regions. The geographical distributions of the emissions adopted in this study are similar to the distributions proposed by *Cooke and Wilson* [1996] and by *Liousse et al.* [1996]. The study by *Black and Kato* [1995] suggests that aircraft fuel combustion is a substantial source of black carbon in the upper troposphere and lower stratosphere. At high latitudes, commercial aircraft usually fly above the tropopause, and a large fraction of the particles are injected into the lower stratosphere. At present, the source of black carbon from aircraft is not included in the model.

Laboratory measurements of heterogeneous reactions occurring on the surface of black carbon suggest that reactions take place primarily on hydrophobic particles [*Golden and Manion*, 1992; *Fendel et al.*, 1995; *Rogaski et al.*, 1997]. However, black carbon is often present as a heterogeneous mixture of carbon, sulfate, and other components whose behavior is hydrophilic [*Ogren*, 1984; *Hagen et al.*, 1992; *Parungo et al.*, 1994; *Liousse et al.*, 1993]. It is believed that black carbon is coated by sulfate and other components, and the initial hydrophobic properties of black carbon are progressively lost as the age of particles increases, and hence the reactivity on elemental black carbon is gradually reduced, as suggested by *DeMore et al.* [1997]. A recent study by *Aumont et al.* [1999] suggests that the reaction of NO_2 on black carbon particles occurs only on the young black carbon particles (hydrophobic carbon). To simulate the heterogeneous reactions occurring on elemental black carbon, we have separated the black carbon particles into two types of aerosols. The first type is assumed to represent new and fresh particles, which are directly emitted from the surface. These particles with high heterogeneous reactivity are assumed to be hydrophobic (i.e., not mixed with other aerosols and not coated by water and acids). These particles are not subject to wet scavenging but are subject to dry deposition with a deposition velocity of 0.1 cm/s as suggested by *Cooke and Wilson* [1996]. For convenience, hydrophobic black carbon is named BC-1. The second type of black carbon particles represent aged particles, that are assumed to be coated with other aerosols including liquid water and sulfates, and therefore, are hydrophilic. With these surface properties the heterogeneous reactivity of the particles is substantially reduced. This type of aerosol is subject to both wet and dry deposition. The removal rate for wet scavenging is assumed to be the same as for sulfate aerosols. For convenience, hydrophilic black carbon particles are named BC-2. BC-2 is not directly emitted, but is converted from BC-1 with a rate of 1 day as suggested by *Cooke and Wilson* [1996].

3. Simulation of Particle Distributions

All the distributions of sulfate and black carbon particles are obtained after 3 years of model integration. Only the results of the last year are used in the present analysis.

3.1. Global Distribution of SO_2 and Sulfate Aerosol Particles

Plate 2 illustrates the surface distributions of gas-phase dimethyl sulfide (DMS) and sulfur dioxide (SO_2), as well as of sulfate aerosols ($SO_4^=$). The calculated surface concentration of SO_2 highlights the large impact of the anthropogenic sources of SO_2 in Europe, Asia, and North America. The SO_2 concentration decreases rapidly away from the source regions due to the short chemical lifetime of SO_2 (~1 day). Over the ocean, where SO_2 is mainly produced by the oxidation of DMS, its concentration is generally less than 100 pptv, i.e., 10 to 100 times smaller than the concentration predicted over the continents. The seasonal variability near the source regions is visible. Because the seasonal cycle of SO_2 emission in the model is relatively small based on IGAC/GEIA [*Benkovitz et al.*, 1994, 1996], the seasonal variation of SO_2 oxidation plays an important role in the calculated seasonal cycle of SO_2 and $SO_4^=$ densities. During winter the chemical sink of SO_2 is low (low OH and H_2O_2 concentrations), and the boundary layer ventilation is weak, leading to high SO_2 and low $SO_4^=$ concentrations. The simultaneous measurements of sulfur emissions, SO_2 and $SO_4^=$ concentrations, in New York and Los Angeles [*Hidy et al.*, 1979] show that SO_2 concentrations are indeed highest during winter, and that sulfate aerosol concentrations are lowest during this season. The distribution of sulfate aerosols however, has a geographic pattern similar to SO_2, suggesting conversion of SO_2 to $SO_4^=$.

A comparison between the calculated and the observed seasonal variation of $SO_4^=$ in Europe and North America is presented in Figure 2a. Table 2 provides the latitude, longitude, and the annual mean concentration at each of these locations. In this region the calculated $SO_4^=$ concentrations are generally within 30% of the observed values except at three locations (Langenbrugge, Ispra, and Union County). A strong seasonal cycle is shown in both the calculated and observed results. During summer the surface $SO_4^=$ is typically high, while during winter it is usually low, suggesting that strong oxidation of SO_2 takes place during summer.

The observed seasonal variation in $SO_4^=$ in the Arctic and sub-Arctic regions (see Figure 2b) is substantially different from the seasonal variability in midlatitude Europe and North America. The maximum concentration occurs in March in contrast to the maximum found in July over Europe and the United States. Since the sulfur emissions at high latitudes are small, SO_2 concentrations are relatively low in these regions (see Plate 2). The direct in situ chemical production of $SO_4^=$ by oxidation of SO_2 is not significant here. $SO_4^=$ particles in the Arctic are therefore originating mainly from midlatitudes and their concentration is likely influenced by the dynamical exchanges between the source regions and the polar regions. The calculated seasonal variability does not reproduce the observations. The calculated maximum often occurs in July, which is ~ 4 months later than the measured maximum. The discrepancy is probably due to differences between CCM and actual winds during the

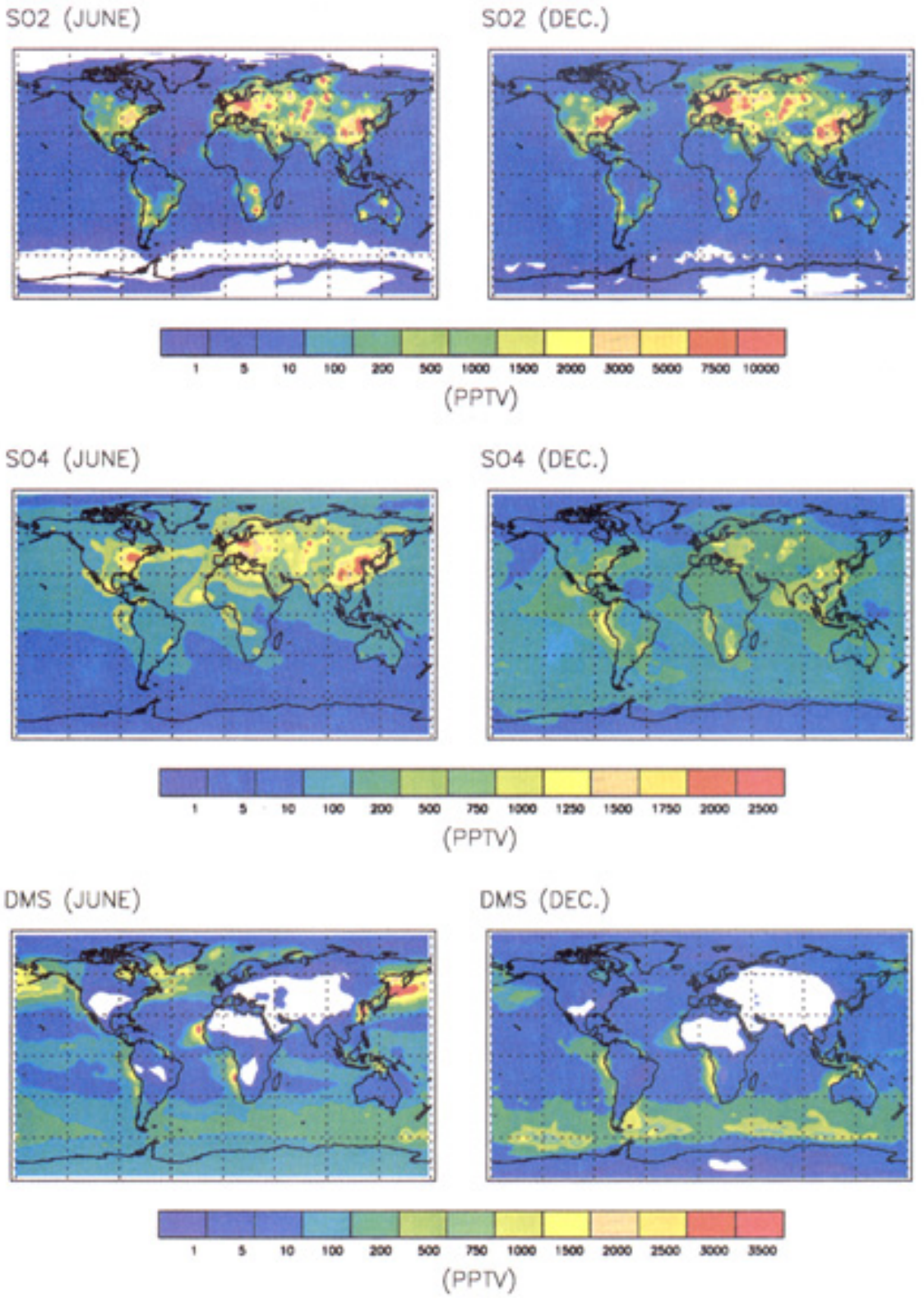

Plate 2. Calculated June and December surface concentrations (pptv) of (top) SO_2, (middle) $SO_4^=$, and (bottom) DMS.

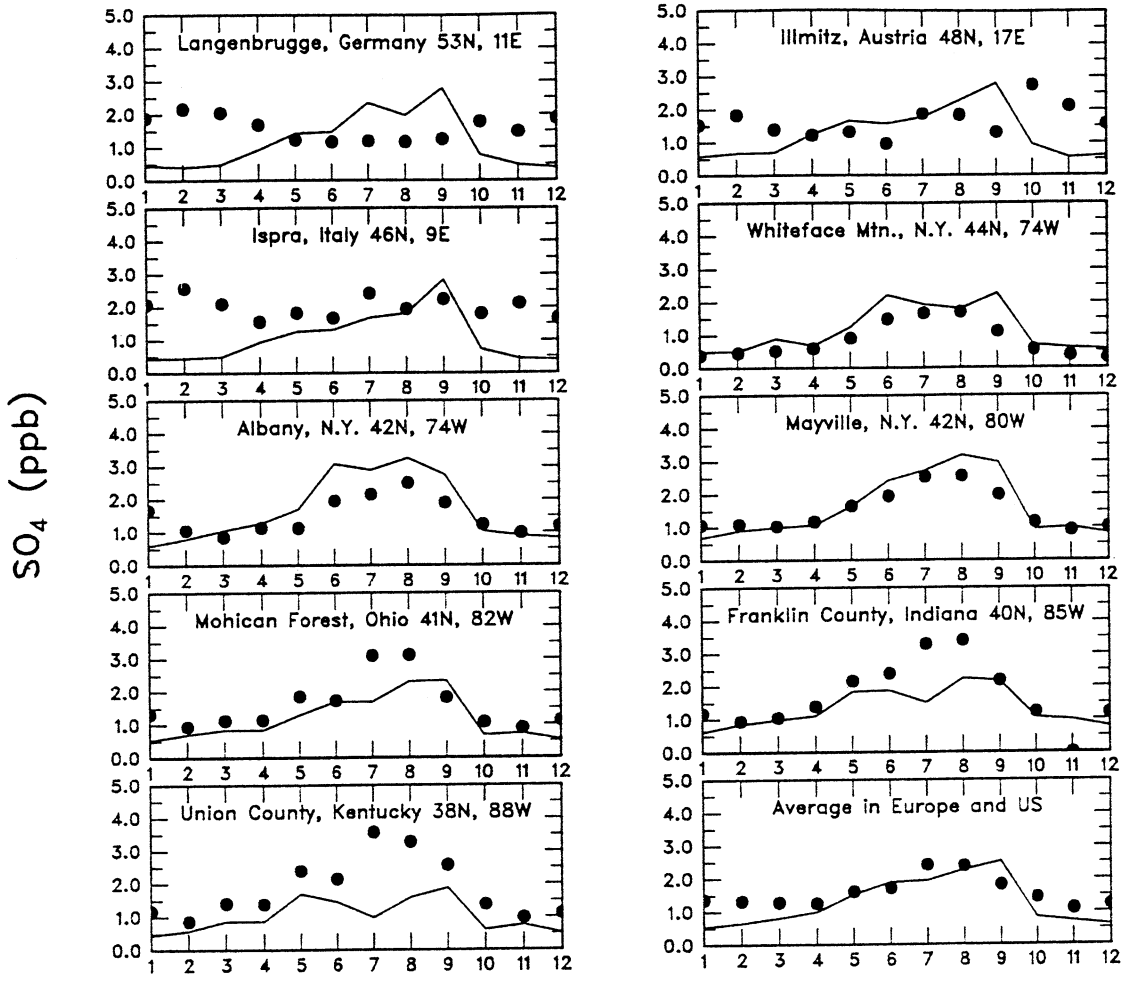

Figure 2a. Monthly-averaged seasonal variation of $SO_4^=$ mixing ratio (ppbv) in Europe and North America. Solid circles are the observations, and solid lines are the model results. Measurements are obtained from *Chin et al.* [1996], and the measurement sites are listed in Table 2.

measurements in the representation of winds by the general circulation model (CCM2).

Over the oceans (Figure 2c), both calculated and measured seasonal variabilities of $SO_4^=$ are not significant, and concentrations are very small (10 times smaller than the values in Europe and the United States) (see Figure 2c). It indicates at these locations, $SO_4^=$ is not significantly affected by transport from polluted source regions. In the Southern Hemisphere at high latitudes, $SO_4^=$ concentrations are high during summer and low during winter, indicating that the seasonal cycle of the oxidizing of DMS has a large effect on $SO_4^=$ over this region. The calculated seasonal variability is generally consistent with the observations, except at two locations (Mace Head and Bermuda) where sulfate aerosols are transported from the polluted European and American continents (see Plate 2).

A comparison between the calculated and the observed seasonal variation of SO_2 is presented in Figure 3. Table 3 provides the latitude, longitude, and the annual mean concentration at each of these locations. The measured SO_2 concentrations are widely spread, ranging from 18 to 8500 pptv. Typical surface concentrations in heavily polluted western Europe and eastern United States range from 3 to 8 ppbv. For relatively clean rural sites of Europe, measured values vary from 0.2 to 0.9 ppbv. The SO_2 concentrations are very low over oceans in the Southern Hemisphere, with mixing ratios of only 18 pptv observed at Amsterdam Island. Such large spatial variations are well reproduced by the model (see Figure 3).

It is shown in Figure 2a and Figure 3 that SO_2 and $SO_4^=$ exhibit strong seasonal cycles in North America, where most measurement sites are near the sources of SO_2. As a result, chemical conversion of SO_2 to $SO_4^=$ plays an important role in controlling the concentrations of SO_2 and $SO_4^=$ at these sites. During summer, OH and H_2O_2 concentrations are highest because of the strong sunlight, resulting in fast chemical conversion of SO_2 to $SO_4^=$. The predicted seasonalities of SO_2 and $SO_4^=$ are consistent with the measurements, with highest concentrations of SO_2 and lowest $SO_4^=$ during winter and lowest concentrations of SO_2 and highest $SO_4^=$ during summer.

Zonally averaged distributions of DMS, SO_2, and $SO_4^=$ are shown in Figure 4 for June and December conditions. DMS exhibits a strong seasonal variation in the vertical distribution at high latitudes. There are two major source regions for DMS, which are the oceans at high latitudes of the northern and southern hemispheres, respectively. Coastal regions around Africa, South America and Indonesia provide additional large sources of DMS (see Plate 1). In these source regions the level of OH and hence

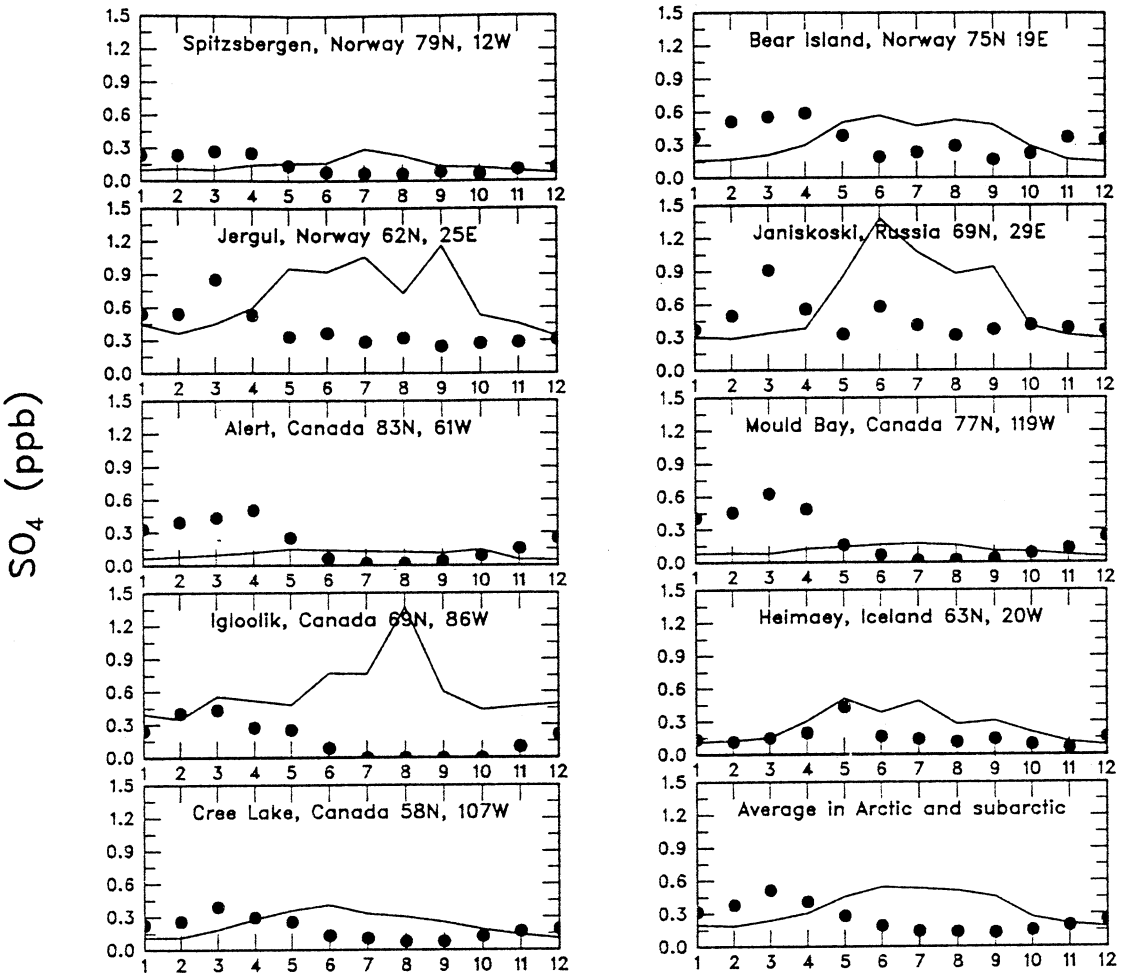

Figure 2b. Same as Figure 2a except in Arctic region.

the destruction rate of DMS vary substantially with season. OH concentrations are highest during summer, resulting in the shortest chemical lifetime of DMS (less than 1 day). The highest DMS concentrations are located in the boundary layer of the source regions, and low concentration values are located in the middle troposphere, where DMS is efficiently removed by OH. During winter, however, OH concentrations are very low, and the chemical destruction is small, so that DMS is more likely to be transported from the boundary layer into the free troposphere. The zonally averaged SO_2 concentration has a maximum in the boundary layer at midlatitudes in the Northern Hemisphere (source region), and decreases rapidly with altitude. The distribution of $SO_4^=$ exhibits less vertical gradient than SO_2 because on the one hand SO_2 concentrations are highest in the boundary layer, and on the other hand, the SO_2 to $SO_4^=$ conversion is facilitated by the cloudiness of the free troposphere. In addition, horizontal and vertical mixing is more extensive for $SO_4^=$ than for SO_2 because the lifetime of $SO_4^=$ (a few days) is larger than the lifetime of SO_2 (1 day). The maximum concentration of $SO_4^=$ located at 45°N in the boundary layer during summer is displaced southward to 25°N during winter because of the shift in the concentration of chemical oxidants (OH and H_2O_2).

Measurements of vertical profiles of sulfur gases are limited, and are far from representing climatologically averaged profiles needed to validate the model. Vertical profiles of SO_2 and $SO_4^=$ were measured during the EMEFS-II and NARE airborne experiments [*Leaitch,* 1998]. The EMEFS-II measurements were obtained from March 22 to April 29, 1990 in Egbert and Lake Traverse (46.3°N, 79.5W) and the NARE samples were collected from August 12 to September 8, 1993 along the east coast of the United States (43.8°N, 66.5W). The number of profiles is relatively large (71 SO_2 profiles and 24 $SO_4^=$ profiles in the case of EMEFS-II, and 46 SO_2 and $SO_4^=$ profiles in the case of NARE). Averaged vertical profiles can reduce or eliminate the effects of mesoscale disturbances which are not represented by the climatological model results. Comparisons between calculated and measured vertical profiles of SO_2 and $SO_4^=$ are shown in Figure 5. During the EMEFS-II experiments, which took place in a polluted continental region, SO_2 concentrations at the surface were very high (6 ppbv), and rapidly decreased with altitude. The calculated vertical profiles are quite consistent with the measurements. However, a large concentration at 6 km (11 ppbv) appears in the measurements, but is not reproduced by the model. This single large concentration may have been associated with a small scale dynamical perturbation such as a strong convection event. The decrease of $SO_4^=$ with altitude is not as rapid as the decrease of SO_2. The measured surface concentration of $SO_4^=$ was ~ 0.25 to 1.0 ppbv, and decreased to 0.25 ppbv at 6 km. The calculated vertical profile of $SO_4^=$ reproduces the observed vertical profile well. In the NARE experiment which was not

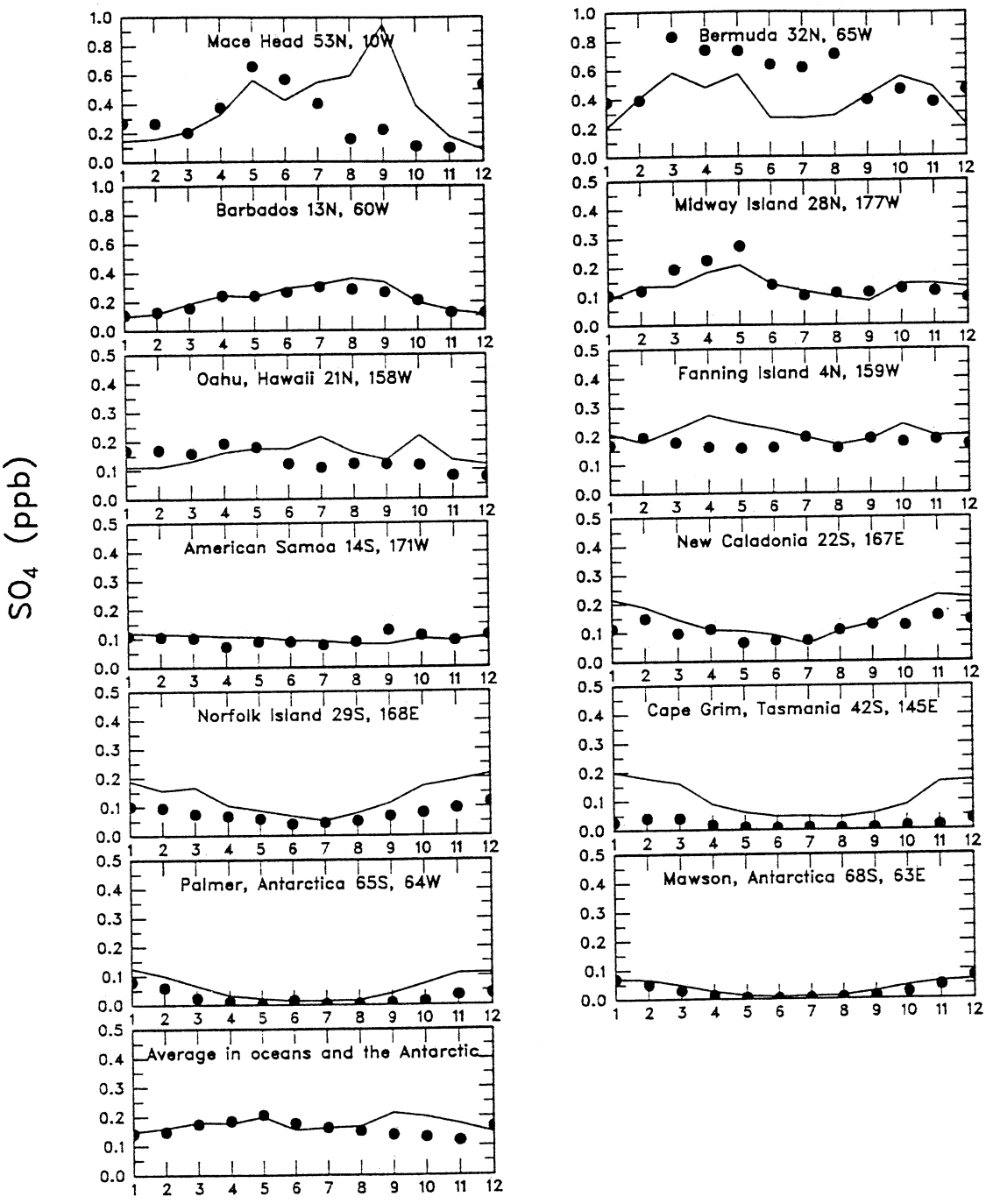

Figure 2c. Same as Figure 2a except over the oceans.

directly located over the source region of SO_2 but was very close to the coast of the United States, the maximum concentrations of SO_2 and $SO_4^=$ appeared in the boundary layer, suggesting that polluted air had been transported from adjacent source regions. Both observed SO_2 and $SO_4^=$ concentrations decreased rapidly with altitude in this region. The calculation reproduces the measurements well, although the calculated maximum of $SO_4^=$ density is slightly larger than the measured value.

3.2. Global Distributions of Black Carbon

The surface distributions of black carbon concentration (ng/m^3) calculated for June and December conditions are shown in Plate 3. As described above, distinguishing between the hydrophobic and hydrophilic particles is important for considering heterogeneous reactions on the surface of the particles. The concentrations of hydrophobic, hydrophilic, and total black carbon are shown in the upper, middle, and lower panels, respectively. Hydrophobic black carbon aerosols are directly emitted at the surface. Because their conversion to hydrophilic black carbon occurs in ~1 day, hydrophobic black carbon particles cannot be transported over a long distance, and therefore remain confined primarily to continental regions. The highest concentration values are well correlated with anthropogenic and biomass burning emissions. Hydrophilic black carbon particles are removed by wet

Table 2. Comparison of the Calculated and the Observed Annually Averaged Surface Sulfate Concentrations[a]

Location	Observed	Calculated
Europe and United States		
Langenbrugge, Germany (53N,11E)	1577.	1158.
Illmitz, Austria (48N,17E)	1639.	1276.
Ispra, Italy (46N,9E)	1915.	1065.
Whiteface Mtn., N.Y. (44N,74W)	1083.	1155.
Albany, N.Y. (42N,74W)	1312.	1678.
Mayville, N.Y. (42N,80W)	1510.	1611.
Mohican Forest, Ohio (41N,82W)	1576.	1183.
Franklin County, Indiana (40N,85W)	1690.	1335.
Union County, Kentucky (38N,88W)	1784.	1022.
Arctic and Subarctic		
Spitzsbergen, Norway (79N,12W))	144.	143.
Bear Island, Norway (75N,19E))	298.	332.
Jergul, Norway (62N,25E)	376.	666.
Janiskoski, Russia (69N,29E)	436.	622.
Alert, Canada (83N,61W)	215.	105.
Mould Bay, Canada (77N,119W)	190.	112.
Igloolik, Canada (69N,86W)	143.	599.
Heimaey, Iceland (63N,20W)	164.	256.
Cree Lake, Canada (58N,107W)	171.	231.
Oceans and Antarctic		
Mace Head (53N,10W)	322.	381.
Bermuda (32N,65W)	560.	393.
Barbados (13N,60W)	204.	219.
Midway Island (28N,177W)	143.	133.
Oahu, Hawaii (21N,158W)	135.	154.
Fanning Island (4N,159W)	174.	211.
American Samoa (14S,171W)	98.	100.
New Caladonia (22S,167E)	112.	149.
Norfolk Island (29S,168E)	75.	133.
Cape Grim, Tasmania (42S,145E)	20.	109.
Palmer, Antarctica (65S,64W)	25.	60.
Mawson, Antarctica (68S,63E)	29.	38.

[a]Concentrations are in pptv.

deposition. Their residence time is on average about a few days which is longer than the lifetime of the hydrophobic carbon particles. As a result, the concentrations of hydrophilic black carbon are higher than those of hydrophobic black carbon. Specifically, the maximum concentration of hydrophilic black carbon is greater than 2000 ng/m^3, while it is ~1000 ng/m^3 in the case of hydrophobic particles. The total concentration of black carbon is therefore heavily weighted towards the hydrophilic particles, although the surface distribution is similar for the two types of particles. The patterns produced by the MOZART model are quite similar to the distributions calculated by *Liousse et al.* [1996]. The model also shows that significant amounts of black carbon are transported from biomass burning sources in both Africa and South America to the remote regions of the tropical Atlantic Ocean, which is consistent with the measurements of *Andreae et al.* [1984]. The seasonal variations are visible for both the hydrophilic and hydrophobic particles. The surface concentrations of black carbon in Europe, eastern United States, and eastern China are higher during winter than during summer because of the seasonal variation in the anthropogenic emissions of black carbon.

Figure 6 shows the vertical and latitudinal distributions of the zonally averaged mass of hydrophobic and hydrophilic black carbon for June and December conditions. The mass of hydrophobic black carbon is largest in the boundary layer, and decreases rapidly in the free troposphere. The heterogeneous reactions associated with black carbon aerosols are therefore limited to the lower troposphere. The model shows that the concentration of hydrophilic black carbon is significant in the lowest levels of the free troposphere although it drops gradually above the boundary layer. Above 10 km, the abundance of black carbon becomes very low as shown experimentally by *Blake and Kato* [1995]. These authors have indicated that the presence of black carbon in the upper troposphere and lower stratosphere results primarily from aircraft emissions. In the tropics, upward motion brings black carbon into the free troposphere. The peak of the black carbon mass concentration is located at 20°S in June, and 20°N in December, as expected from the seasonal variation in convective activity.

Table 4 compares measured and calculated black carbon mass concentrations for ocean and continental sites, respectively. The data are divided into four groups (continental rural, continental remote, Atlantic ocean, and Pacific ocean sites) as suggested by *Liousse et al.* [1996]. Because the observations are often single measurements in which large variations associated with small scale perturbations are exhibited, some disagreement between the model and measurements is expected. The comparison of model calculations with observations is generally consistent: both the calculated and measured total black carbon masses are highest (> 1000 ng/m^3) in the regions of anthropogenic sources (Northern Hemisphere), and lowest (< 1 ng/m^3) in the Antarctic region.

The measured data points shown in Table 4 are plotted against the calculated values in the upper panel of Figure 7. From this comparison, we see that the model values are quite well correlated with the observations, especially when the mass of black carbon is large. However, when the mass of black carbon is low, the correlation is weaker. The lower panel represents the observation-calculation relationship for the four groups of sites (Atlantic Ocean, Pacific Ocean, continental rural, and continental remote). This comparison reveals a systematic difference between observed and calculated values in each individual group; probably associated with the crude resolution of the global model (see Plate 1). Over the ocean the calculated mass of black carbon is higher than the observed values, perhaps due to the fact that observation sites over the ocean are often located in coastal areas. The ocean grid boxes of the model located near the coasts are often contaminated by continental sources, producing an overestimation of the black carbon mass. Similarly, grid cells located in rural continental areas are often affected by local air pollution sources. In a model with limited spatial resolution the averaged emission rates within a grid cell underestimate the emissions near the source regions and overestimate the emissions in the coastal regions. An underestimation of black carbon emissions in

Table 3. Comparison of the Calculated and the Observed Annually Averaged Surface SO_2 Concentrations[a]

Location	Observed	Calculated
Langenbrugge, Germany (53N,11E)	4884.	7306.
Illmitz, Austria (48N,17E)	8029.	7486.
Ispra, Italy (46N,9E)	3485.	4520.
Mohican Forest, Ohio (41N,82W)	7978.	4858.
Franklin County, Indiana (40N,85W)	8523.	8055.
Union County, Kentucky (38N,88W)	7516.	5247.
Spitzsbergen, Norway (79N,12W)	157.	37.
Bear Island, Norway (75N,19E)	205.	207.
Jergul, Norway (62N,25E)	699.	2417.
Janiskoski, Russia (69N,29E)	899.	1654.
Cree Lake, Canada (58N,107W)	242.	347.
Amsterdam Island (38S,78E)	18.	7.

[a]Concentrations are in pptv.

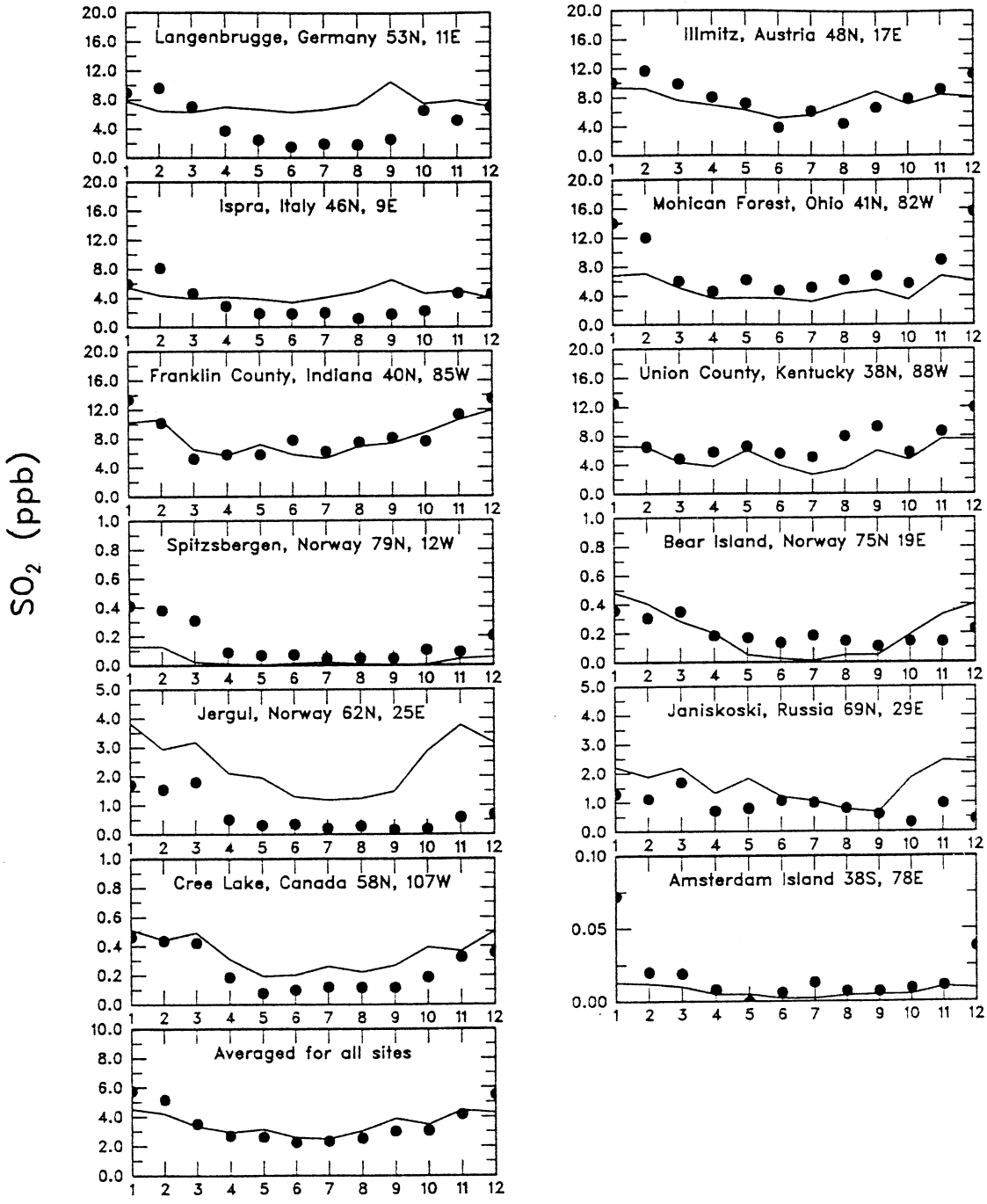

Figure 3. Monthly-averaged seasonal variation of SO_2 mixing ratio (ppbv). Solid circles are the observations, and solid lines are the model results. Measurements are obtained from *Chin et al.* [1996], and the measurement sites are listed in Table 3.

continental rural regions was noted by *Liousse et al.* [1996] in their model calculations.

4. Effects of Heterogeneous Reactions on Tropospheric Chemical Compounds

4.1. Implementation of Heterogeneous Reactions

Heterogeneous chemical kinetics and its application to the troposphere is a relatively new and a rapidly developing field. Currently, more than 40 reactions occurring in various aerosol particles are listed in the compilation of chemical reactions established by *DeMore et al.* [1997]. It is therefore important to determine which heterogeneous reactions are likely to occur on the surface of aerosols, and have the potential to affect tropospheric composition. This requires that the probability of occurrence (uptake coefficient) of potentially important reactions be sufficiently high.

According to *DeMore et al.* [1997], the measured uptake coefficient (γ) is between 0.1 and 1.0 for HO_2 on sulfate aerosols. However, *Mozurkewich et al.* [1987] show that only when sulfate

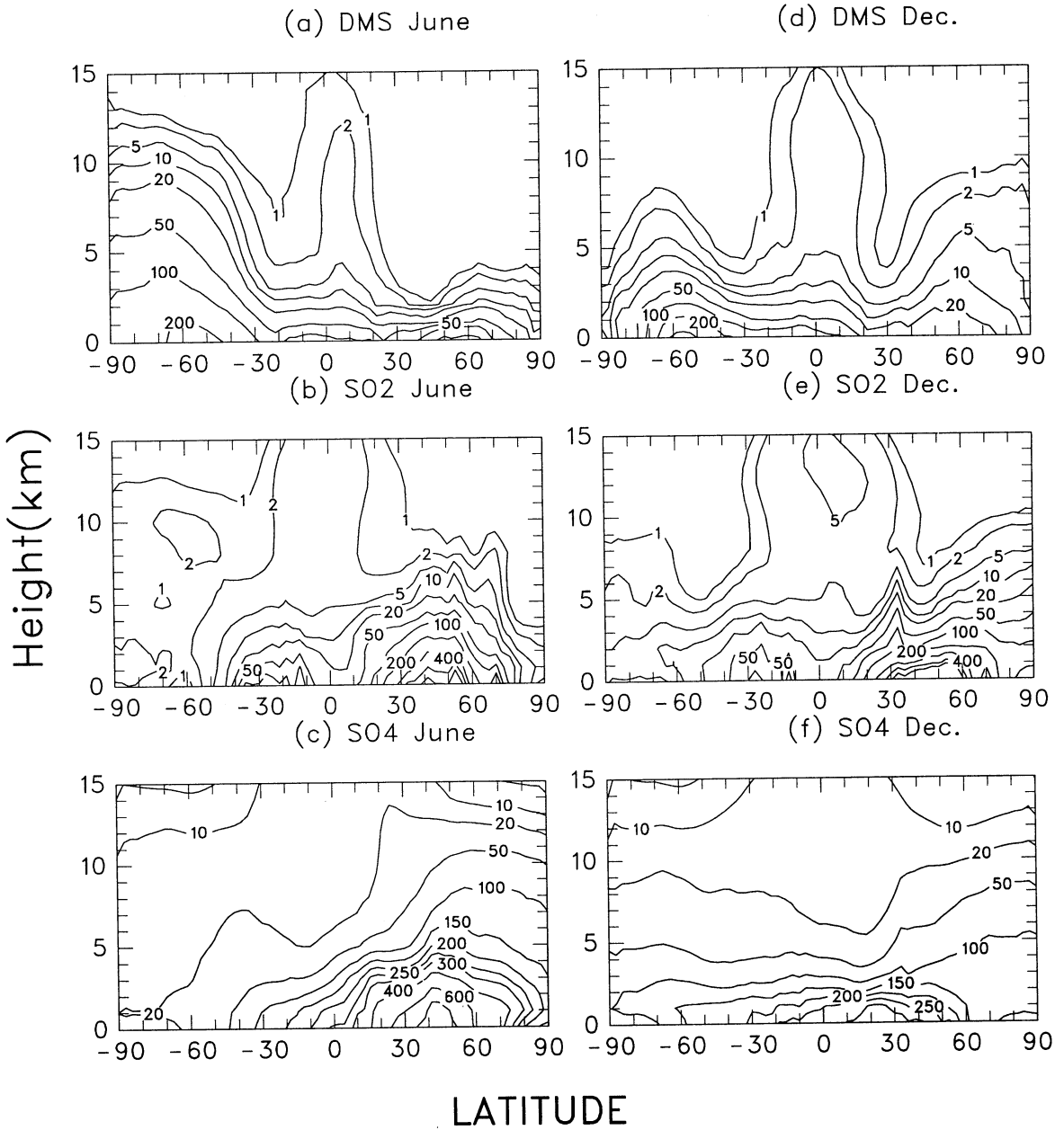

Figure 4. Zonal-averaged mixing ratios (pptv) of (top) DMS), (middle) SO_2, and (bottom) $SO_4^=$ in June and December conditions.

aerosols contained a sufficient amount of Cu ions, reaction of HO_2 with sulfate aerosols was observed. Otherwise, the reaction of HO_2 with sulfate aerosols was not important for atmospheric conditions. The reaction of N_2O_5 on sulfate aerosol which produces HNO_3 has been measured by several groups who have found values of γ ranging from 0.02 to 0.20 [*Van Doren et al.*, 1991; *Hanson and Ravishankara,* 1992; *Fried et al.*, 1994; *George et al.*, 1994; *Hanson and Lovejoy*, 1994; *Zhang et al.*, 1995; *Robinson et al.*, 1997]. The lowest uptake coefficient is observed by *George et al.* [1994], who report values decreasing from 0.03 to 0.013 with the increasing in temperature. The study by *Hu and Abbatt* [1997] shows that the uptake coefficient of N_2O_5 is a function of relative humidity (RH) and ionic composition. For low RH the uptake coefficient on sulfate aerosols varies from 0.05 to 0.06, while for higher RH it decreases to 0.02. The uptake of gas-phase formaldehyde, CH_2O, by sulfate aerosols has been measured by *Jayne et al.* [1996]. Their measurement shows that the uptake coefficient for CH_2O by sulfate aerosols ranges from 0.012 to 0.025 when the weight percentage of sulfate varies from 55 to 70% and the temperature changes from 240K to 280K. Their measurement should be regarded as solubility-determined upper limits.

The reactions of HNO_3, O_3, and NO_2 on the surface of soot have been measured in a number of laboratory experiments, and the measured values are very different from each other. The rate at which HNO_3 reacts on black carbon (HNO_3+BC) to produce NO_x has been measured by *Thlibi and Petit* [1994], *Rogaski et al.* [1997], *Choi and Leu* [1998], and *Saathoff et al.* [1999]. The measurements by *Thlibi and Petit* [1994] and *Rogaski et al.* [1997] suggest that the uptake coefficient γ is of the order of 10^{-2}.

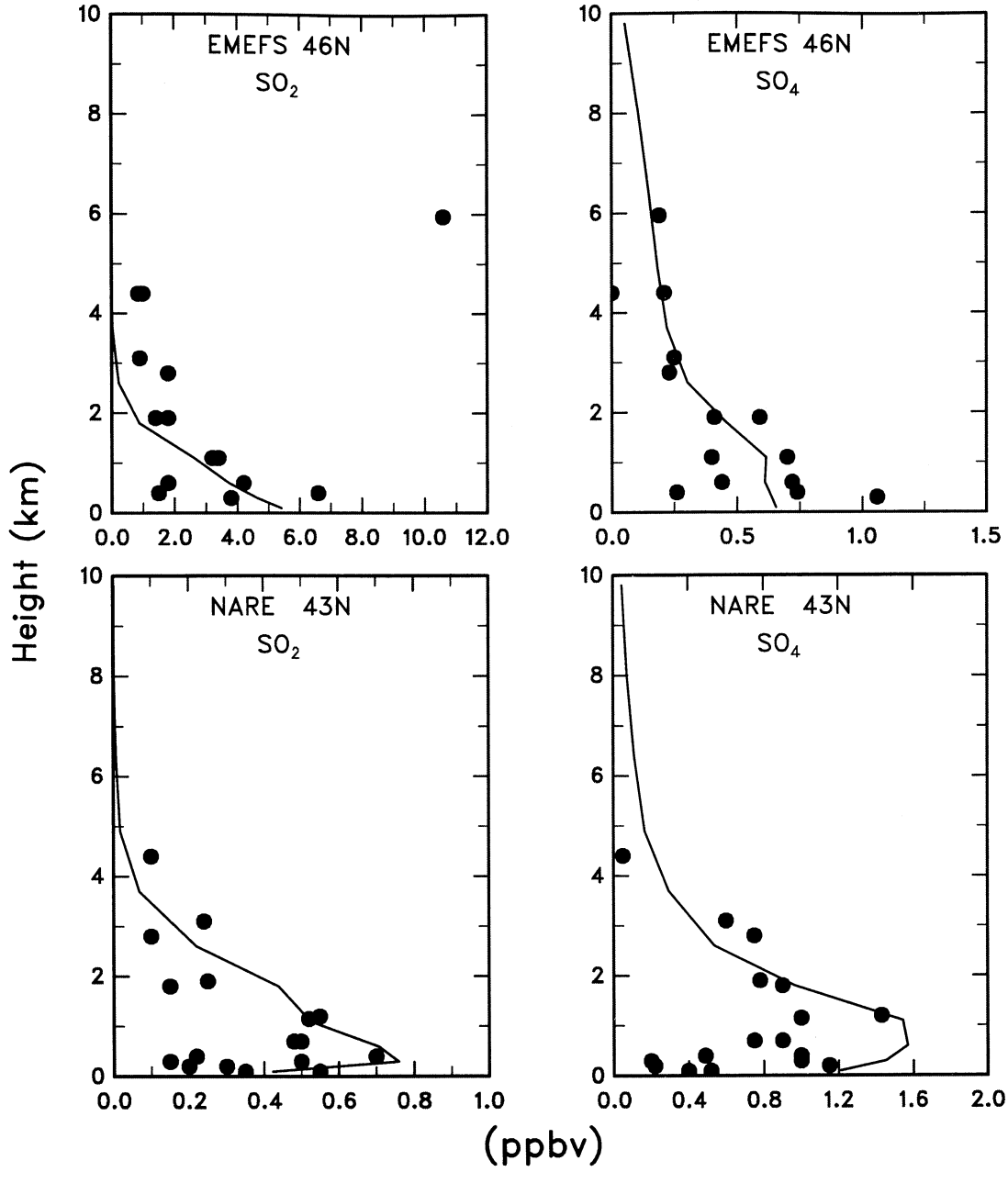

Figure 5. Vertical profiles of SO_2 and $SO_4^=$ for the (top) EMEFS and the (bottom) NARE measurements [*Leaitch*, 1998]. Solid lines are the model results, and solid circles are the observations.

However, *Choi and Leu* [1998] show that the decomposition of HNO_3 to NO_x does not take place at 220K but does occur at 296K. Their results suggest that the heterogeneous conversion of HNO_3 to NO_x on soot should not be included in atmospheric models of the upper troposphere and of the lower stratosphere. The recent measurement by *Saathoff et al.* [1999] shows that the coefficient is much smaller than derived from the previous measurements and is probably of the order of 10^{-6}.

The various measurements for the uptake of O_3 on soot particles are also very scattered. *Fendel et al.* [1995], *Fendel and Ott* [1993], and *Rogaski et al.* [1997] report that O_3 reacts on black carbon particles with an uptake coefficient ranging from 2 x 10^{-4} to 3.3 x 10^{-3}, but the recent study by *Saathoff et al.* [1999] shows that the uptake coefficient is only on the order of 10^{-5}. *Saathoff et al.* [1999] argue that the reason for the smaller reaction coefficients for HNO_3 and O_3 on soot surface is that their measurements address the heterogeneous processes on a longer timescale (hours).

Tabor et al. [1993], *Rossi et al.* [1995], and *Rogaski et al.* [1997] report that NO_2 can react on the surface of soot particles, with an uptake coefficient ranging from 0.04 to 0.11, but a recent measurement by *Kleffmann et al.* [1999] shows that the uptake coefficient is only of the order of 10^{-6}. As suggested by *Aumont et al.* [1999], the sites on the surface of soot may be deactivated as a result of NO_2 reactions. Therefore the high initial rates of the reactions do not persist for long timescales. The large scatter in

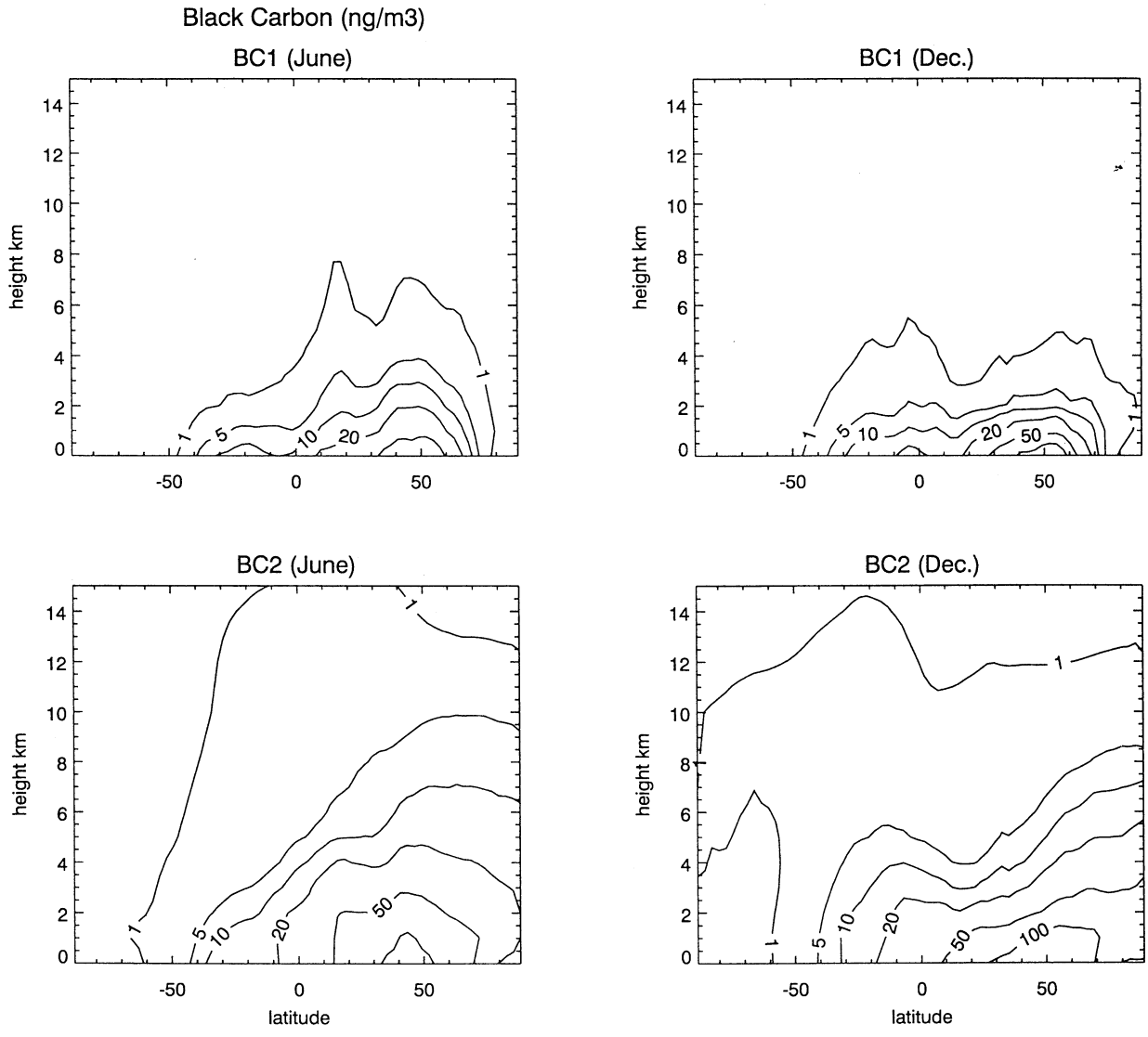

Figure 6. Zonally averaged mixing ratios (pptv) of (top) hydrophilic black carbon and (bottom) hydrophobic black carbon in June and December.

the data reported for these reactions points to the need for further laboratory studies. *Longfellow et al.* [1999] and *Goodman et al.* [1999] discuss the heterogeneous reaction of NO_2 on soot particles, which is believed to produce HONO. HONO chemistry is not included in the MOZART model, and therefore this heterogeneous reaction will not be considered in the present study.

Considering the large uncertainty associated with the heterogeneous reactions, we have conducted the following studies to estimate the potential effects of aerosols on atmospheric chemical constituents: (1) The measured uptake coefficient for HO_2 and OH on sulfate aerosols ranges from 0.1 to 1.0 [*DeMore et al.*, 1997]. In this study we arbitrarily chose the uptake coefficient to be 0.2 and 0.5. According to the study by *Mozurkewich et al.* [1987], these values should be regarded as upper limit. (2) The reaction coefficient for N_2O_5 on sulfate aerosols is less uncertain, so that $\gamma = 0.1$ is used in the model. (3) The measured reaction coefficient for CH_2O on sulfate aerosols ranges from 0.011 to 0.022 [*Jayne et al.*, 1996] so that we use the value of 0.011 as an lower limit and 0.022 as a upper limit. (4) The measured reaction coefficients on soot particles differ by several orders of magnitude. We will consider the calculated effects of reactions on soot aerosols solely in sensitivity studies. We have used the uptake coefficient of 3.3×10^{-3} as an upper limit value and 7×10^{-5} as a lower limit value for the reaction O_3 on hydrophobic soot. The heterogeneous reactions included in the model are therefore the following:

(R12) $HO_2 + (SF) \rightarrow$ products,
(R13) $N_2O_5 + (SF) \rightarrow 2HNO_3$,
(R14) $CH_2O + (SF) \rightarrow$ products,
(R15) $O_3 + (soot) \rightarrow$ products,

where SF and soot represent the surface of sulfate and soot aerosols, respectively. In reactions of(R12), (R14), and (R15) the reaction products are unknown according to current laboratory measurements. In our model calculations those reactions are considered as chemical losses for the reactants. This assumption

Table 4a. Comparison of the Calculated and the Observed Black Carbon (BC1+BC2) Surface Concentration at Ocean Sites

Location	Concentration ng C/m^3 Observed	Calculated
Atlantic Ocean		
North Atlantic 1 (68.0N, 8.0W)	112.0	100.9
North Atlantic 2 (42.5N, 14.0W)	50.0	84.9
North Atlantic 3 (20.0S, 40.0W)	30.0	146.2
Bermuda (32.2N, 64.5W)	60.0	60.9
Sargasso Sea (30.0N, 50.0W)	20.0	47.5
Pacific Ocean		
Pacific 1 (45.0N, 160.0W)	20.0	14.4
Pacific 2 (20.0N, 160.0W)	7.0	19.4
Pacific 3 (0, 160.0W)	3.0	11.0
Pacific 4 (20.0S, 160.0W)	8.0	3.1
Mauna Loa (19.3N, 155.4W)	7.5	25.4
East Pacific (0, 120.0W)	10.0	10.9
Pacific 5 (30.0N, 128.0E)	355.0	320.1
Pacific 6 (30.0N, 125.0E)	505.0	529.6
Pacific 7 (30.0N, 126.0E)	133.0	362.6
Pacific 8 (10.0N, 165.0E)	25.0	3.9
Enewetak (11.3N, 162.1E)	50.0	11.9
China Sea (10.0N, 113.0E)	33.0	71.3
West Pacific (0, 150.0E)	9.0	9.6
Samoa (13.6S, 172.0W)	19.0	3.6

will result in an overestimate of the chemical loss if the products regenerate the chemical reactants.

Most chemical species removed by heterogeneous reactions can also be lost through gas-phase reactions. If gas-phase removal is fast, heterogeneous reactions are unlikely to play a significant role. The lifetime associated with heterogeneous reactions τ_{het} is provided by the inverse of the pseudo first-order heterogeneous rate constant [*Schwartz*, 1986]:

$$k_{het} = [r/Dg + 4/(c\gamma)]^{-1} A \times 10^{-8}, \quad (1)$$

where $c = [8kT/\pi m]^{1/2}$ (cm/s) is the mean molecular speed of the gas at temperature T, A ($\mu m^2/cm^3$) is the surface area density of the particles, γ is the uptake coefficient, m (g) is the molecular mass of the gas-phase molecule under consideration, k is the Boltzmann constant, D_g (cm^2/s) is the gas-phase diffusion coefficient, and r is the mean radius of the aerosol particles. According to the calculation of *Perry and Green* [1984], D_g is close to 0.1 cm^2/s.

Figure 8 compares the characteristic time constant for the heterogeneous reaction OH+SF (uptake coefficient $\gamma = 0.2$) with the time constant due to gas-phase loss reactions. Figure 8 shows that although the heterogeneous destruction of OH is relatively fast (τ_{het} is ~ 1000 seconds at northern midlatitudes near the surface), it can be neglected compared to gas-phase photochemical destruction (τ_{gas} = 1 to 2 s).

To study the heterogeneous reactions on the surface of aerosols requires that the surface area of aerosols be known. The aerosol quantity that is calculated in the model is the aerosol mass. To convert mass to surface area, the mean radius of the aerosol particles must be determined or assumed. The measured properties of sulfate and black carbon particles are summarized by *Blake and Kato* [1995]. Their study suggests that the average radius is ~ 0.1 μm in the case of black carbon particles, and ~ 0.15 μm in the case of sulfate aerosols. Because the detailed microphysical processes of aerosols are not included in the model, the size distribution of aerosols is unknown. To convert the mass into surface area, we assume that (1) aerosols are spherical, and (2) a mean radius is used to represent the detailed size distribution. With these assumptions, the aerosol surface area density ($\mu m^2/cm^3$) can be calculated from the aerosol mass (g/cm^3) as follows:

$$\text{Area} = 3\ \text{Mass}/(\rho r_m) \times 10^8, \quad (2)$$

where ρ (g/cm^3) is the mass density of the aerosol, r_m (cm) is mean radius, and Mass is the total mass. Black carbon aerosol density is assumed to be 2.0 g/cm^3 [*Blake and Kato*, 1995], and sulfate aerosol density is calculated according to the weight percentage of sulfuric acid [*Tie et al.*, 1994a]. However, the spherical assumption cannot be applied to black carbon. Typical geometries for these particles range from compact spheroidal shapes to chain aggregates [*Blake and Kato*, 1995]. With the same aerosol mass, different shapes of particles result in very different aerosol surface areas. To account for this effect, *Blake and Kato* [1995] assume that a particle of black carbon is a cluster of small spherical particles (0.02 μm in radii). From (2) we see that the surface area of a cluster of small spherical particles is 5 times larger than the surface area calculated for larger spherical particles (0.1 μm radius), for the same total mass.

Figure 9 shows the zonally averaged surface area densities ($\mu m^2/cm^3$) calculated for sulfate, black carbon, and hydrophobic black carbon in June, indicating that the highest sulfate surface area density is located in the boundary layer of the Northern Hemisphere midlatitudes with a maximum value of above 50

Table 4b. Comparison of the Calculated and the Observed Black Carbon (BC1+BC2) Surface Concentration at Continental Sites

Location	Concentration ng C/m^3 Observed	Calculated
Rural Sites		
Mace Head (53.3N, 9.8W)	168.5	153.2
Florida (28.0N, 82.0W)	400.0	342.1
SouthWest (34.3N, 106.0W)	185.0	188.0
North Carolina (35.3N, 80.0W)	520.0	532.2
Abisko (68.2N, 18.3E)	520.0	371.2
Hemsby (52.4N, 1.4E)	466.0	380.2
Abstumani (41.4N, 42.5E)	980.0	743.2
Dogo (36.2N, 133.2E)	623.0	719.8
Isenbai (38.3N, 68.4E)	1000.0	475.4
BeJing (40.0N, 116.0E)	1710.0	1144.6
Lin An (30.5N, 119.5E)	2070.0	1051.1
Ecuador (2.0S, 77.3W)	310.0	196.0
Brazil (10.0N, 55.0W)	410.0	333.5
Peru (10.0S, 76.0W)	24.0	20.2
Cape Grim (40.7S, 144.4E)	3.0	13.1
Remote Sites		
Greenland (70.0N, 40.0W)	30.0	28.9
Barrow (71.2N, 156.3W)	43.0	43.6
Arctic Point (74.0N, 25.0E)	148.0	208.1
Spitsbergen (79.0N, 12.0E)	66.0	57.6
Alert Summer (82.5N, 62.5W)	15.0	18.1
Alert Winter (82.5N, 62.5W)	75.0	86.4
Amsterdam Island (37.5N, 77.3E)	5.5	5.5
New Zealand (41.0S, 174.0E)	2.2	6.1
Halley Bay (75.4S, 27.0W)	1.7	.7
South Pole 1 (87.0S, 102.0W)	.3	.6
South Pole 2 (87.0S, 102.0W)	1.3	.6

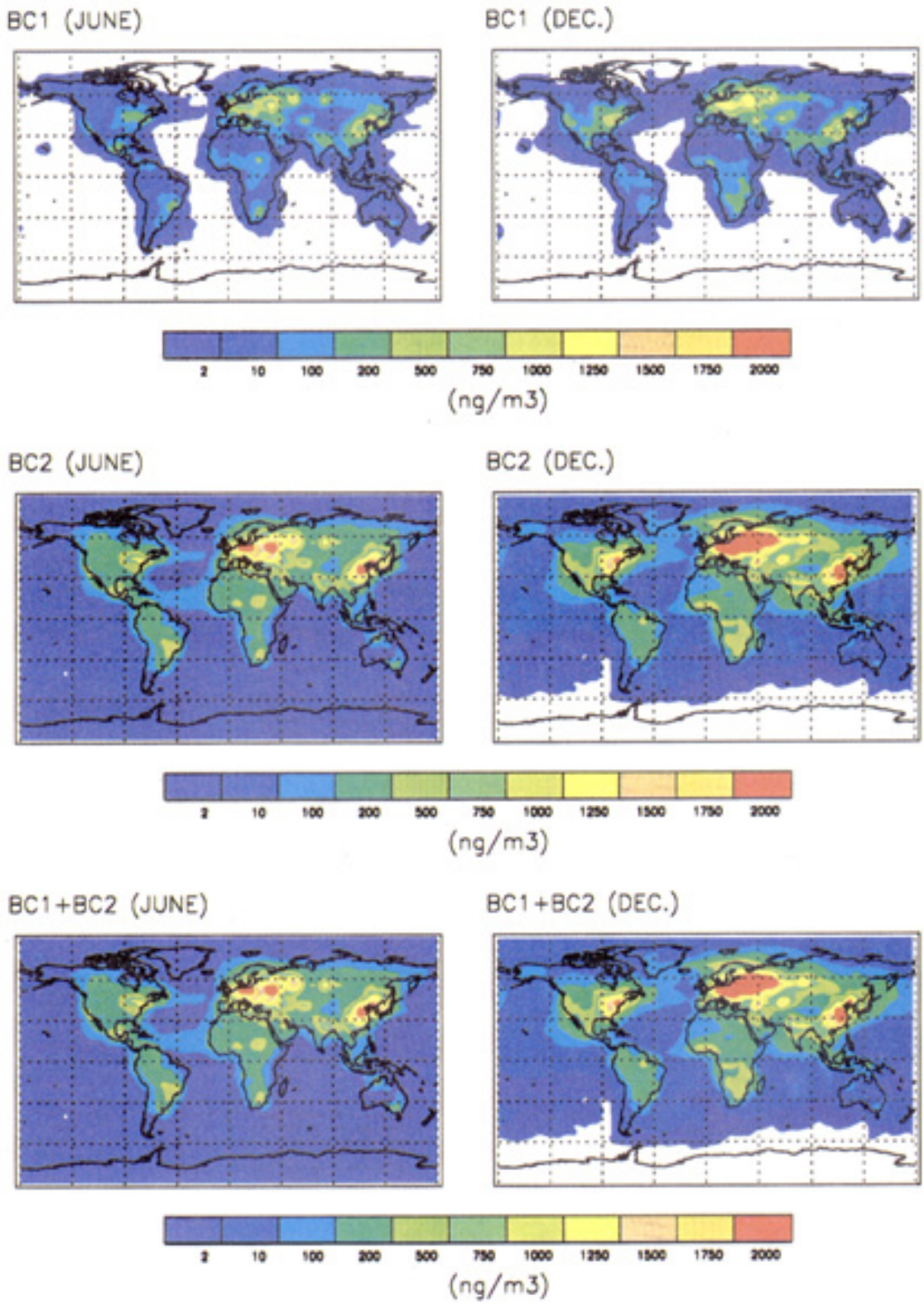

Plate 3. June and December surface mixing ratios (pptv) of (top) hydrophobic black carbon, (middle) hydrophilic black carbon, and (bottom) total black carbon.

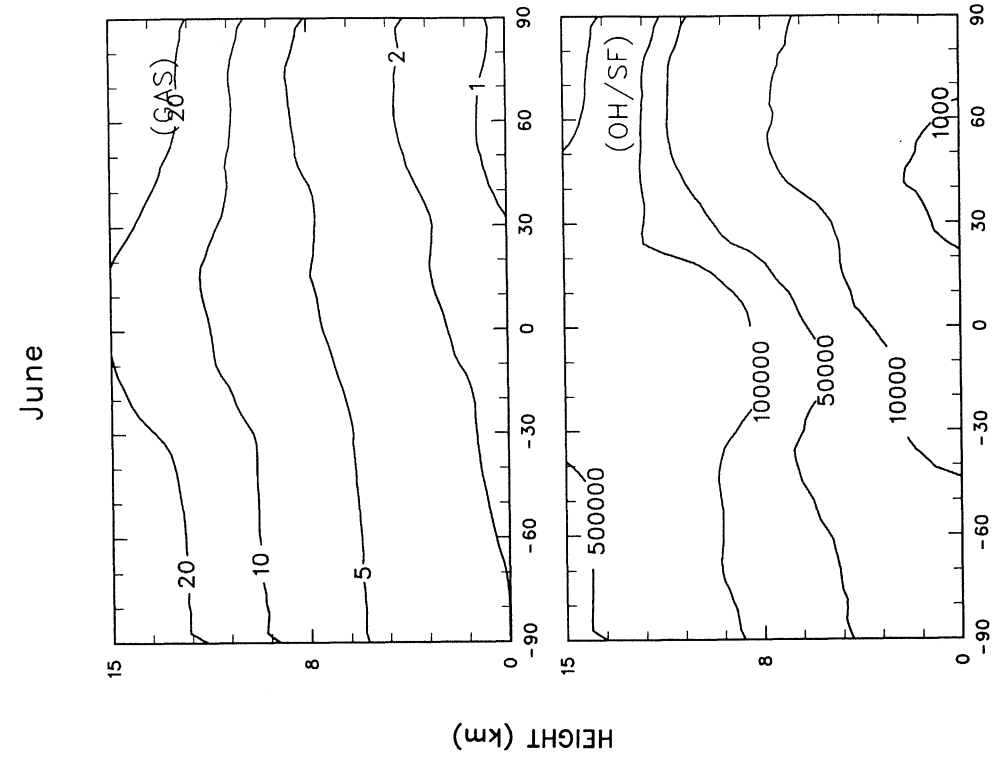

Figure 8. (top) Zonally-averaged lifetime of OH (seconds) due to gas-phase chemical destruction and heterogeneous chemical destruction on sulfate aerosol particles in June.

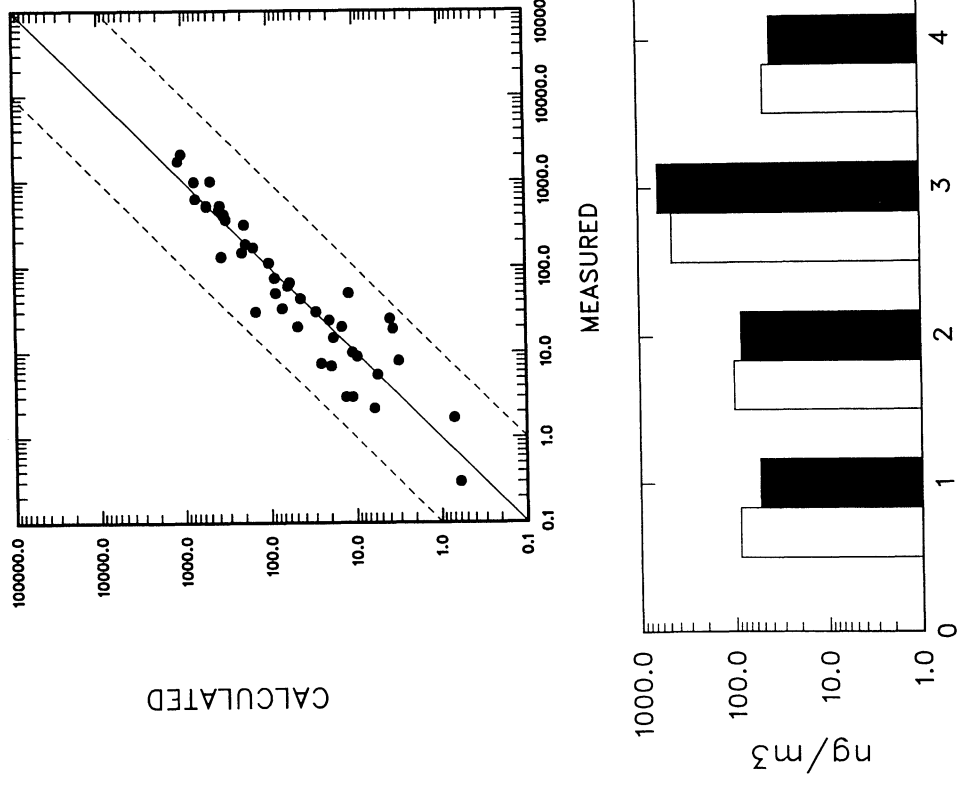

Figure7. (top) Observed versus calculated black carbon mixing ratios (ng/m^3). Solid line denotes the one-to-one correspondence between model and observations; dotted lines denote a factor of ten departure. The data are given in Table 4 [*Liousse et al.*, 1996]. (bottom) Observed versus calculated black carbon mixing ratios averaged in four groups (1, Atlantic ocean; 2, Pacific ocean sites; 3, continental rural; and 4, continental remote). Solid bars are the observations and open bars are the model results.

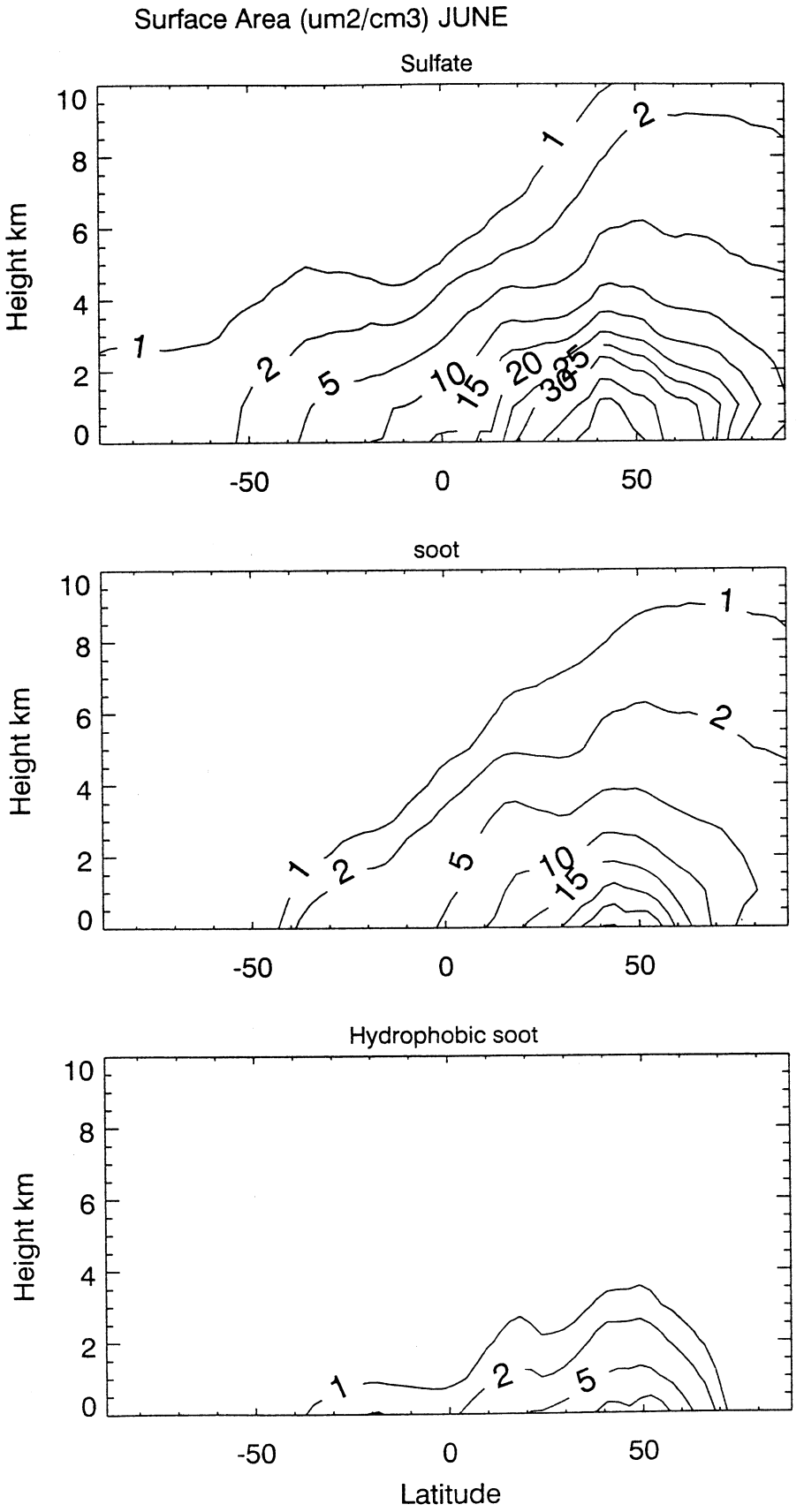

Figure 9. Zonally-averaged surface areas of (top) sulfate aerosols ($\mu m^2/cm^3$), (middle) total black carbon aerosols, and (bottom) hydrophobic black carbon aerosols in June.

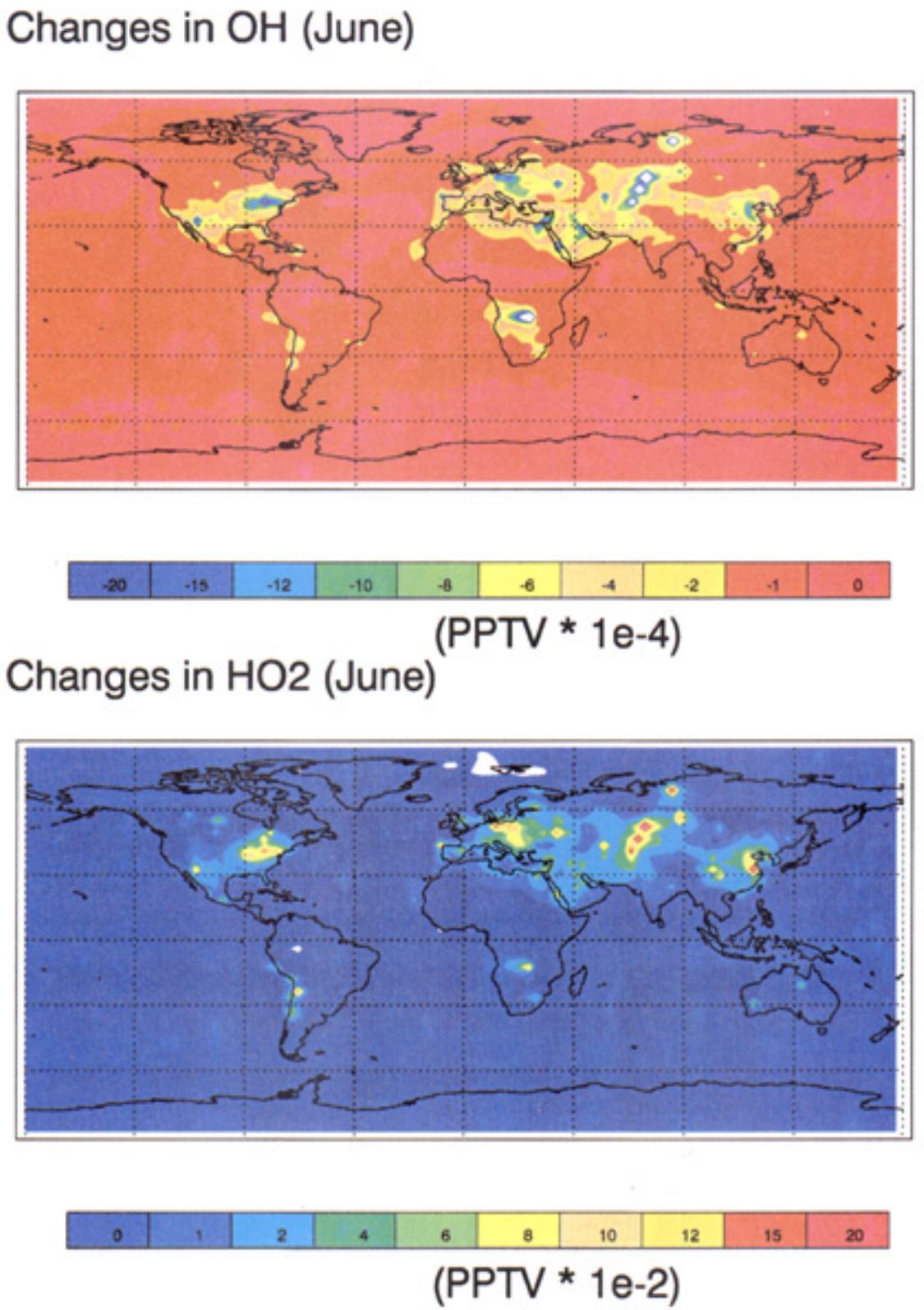

Plate 4. Changes in (top) OH and (bottom) HO_2 at the surface due to the formation of sulfate aerosols in June.

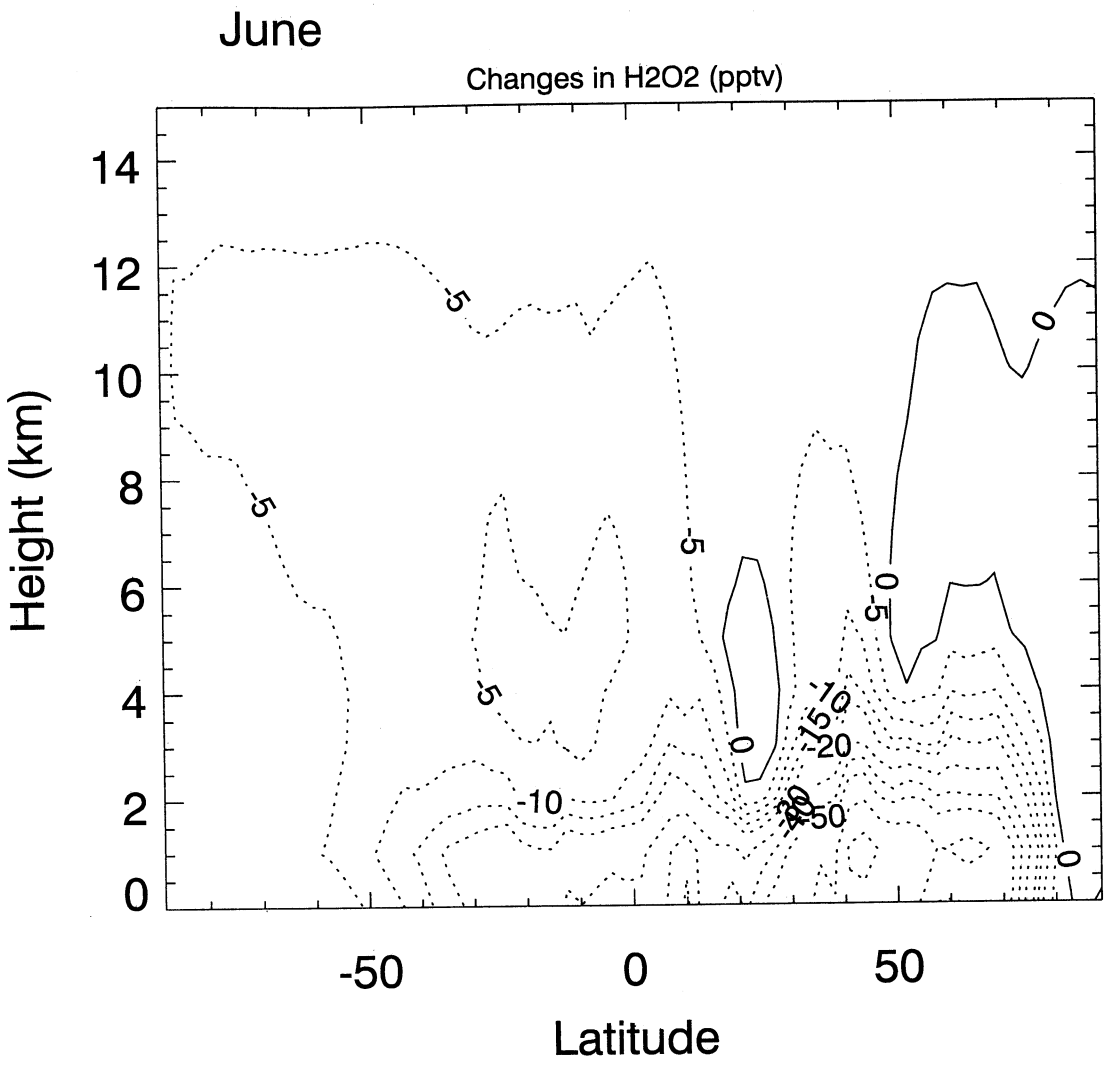

Figure 10. Zonally-averaged changes in H_2O_2 (pptv) due to the formation of sulfate aerosols in June.

$\mu m^2/cm^3$. The area density decreases rapidly with altitude. The surface area of black carbon has a geographical distribution similar to sulfate aerosols at midlatitudes in the Northern Hemisphere. However, a secondary maximum associated with biomass burning in the tropics is also visible. The highest values in the boundary layer of the northern midlatitudes are close to 30 $\mu m^2/cm^3$ and hence are smaller than in the case of sulfate aerosols. As described in section 2.5, heterogeneous reactions on black carbon are only occurring on the surface of hydrophobic particles. Figure 9 shows that the surface area density of the hydrophobic black carbon particles is substantially smaller than either of sulfate or hydrophilic black carbon particles. The highest surface area is ~10 $\mu m^2/cm^3$ near the surface at midlatitudes in the Northern Hemisphere, and is well confined to the lower troposphere. The emissions from aircraft in the upper troposphere are not included in the present model study, so that the surface area of hydrophobic black carbon is probably underestimated in the upper troposphere.

4.2. Effects of Oxidation of Sulfate Aerosols

The concentrations of oxidants is changed when chemical conversion of SO_2 to $SO_4^=$ occurs. The oxidants (OH, HO_2, and H_2O_2) are affected in the following ways: (1) Gas-phase OH is converted to HO_2 through the reaction of SO_2 + OH. As shown in Plate 4 (top) the largest reduction in the OH concentration occurs during northern summertime in the regions that are most heavily influenced by anthropogenic emissions of sulfur (eastern United States, Europe, and eastern China). As a result, the concentration of HO_2 increases in the same regions (see Plate 4 (bottom)). However, the changes in OH and HO_2 due to this reaction are very small (less than a few percent). (2) The oxidation of SO_2 by H_2O_2 in the aqueous phase tends to reduce the H_2O_2 abundance in the gas phase. Figure 10 shows that the reduction in the H_2O_2 mixing ratio ranges from 5 to 60 pptv in the Northern Hemisphere during summer. In areas with high sulfur emissions (eastern United States, Europe, and eastern China), this H_2O_2 reduction is ~ 5 to 10%. Overall, the calculation shows that the effect of SO_2 oxidation on the oxidants (OH, HO_2, and H_2O_2) in the troposphere is not very significant.

4.3. Reaction of HO_2 on Sulfate Aerosols

Even though the uptake of OH by sulfate aerosol is very efficient ($\gamma > 0.2$), the direct changes in the OH concentration resulting from heterogeneous processes are small due to the short

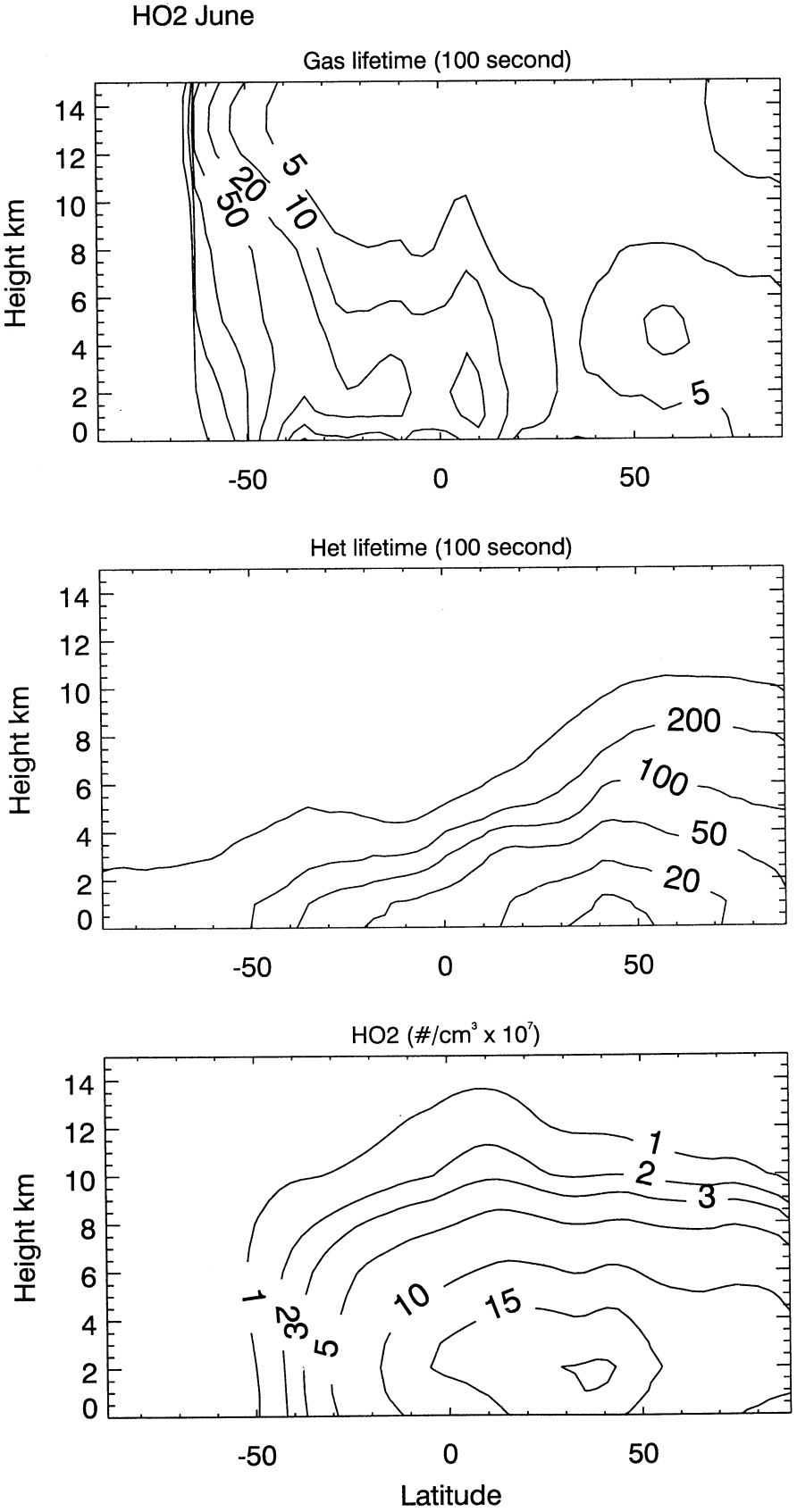

Figure 11. (top) Zonally-averaged time constants of HO_2 (100 s) due to gas-phase chemical destruction and (middle) heterogeneous chemical destruction on sulfate aerosol particles. (bottom) The number density of HO_2 (#/cm^3 x 10^7) in June.

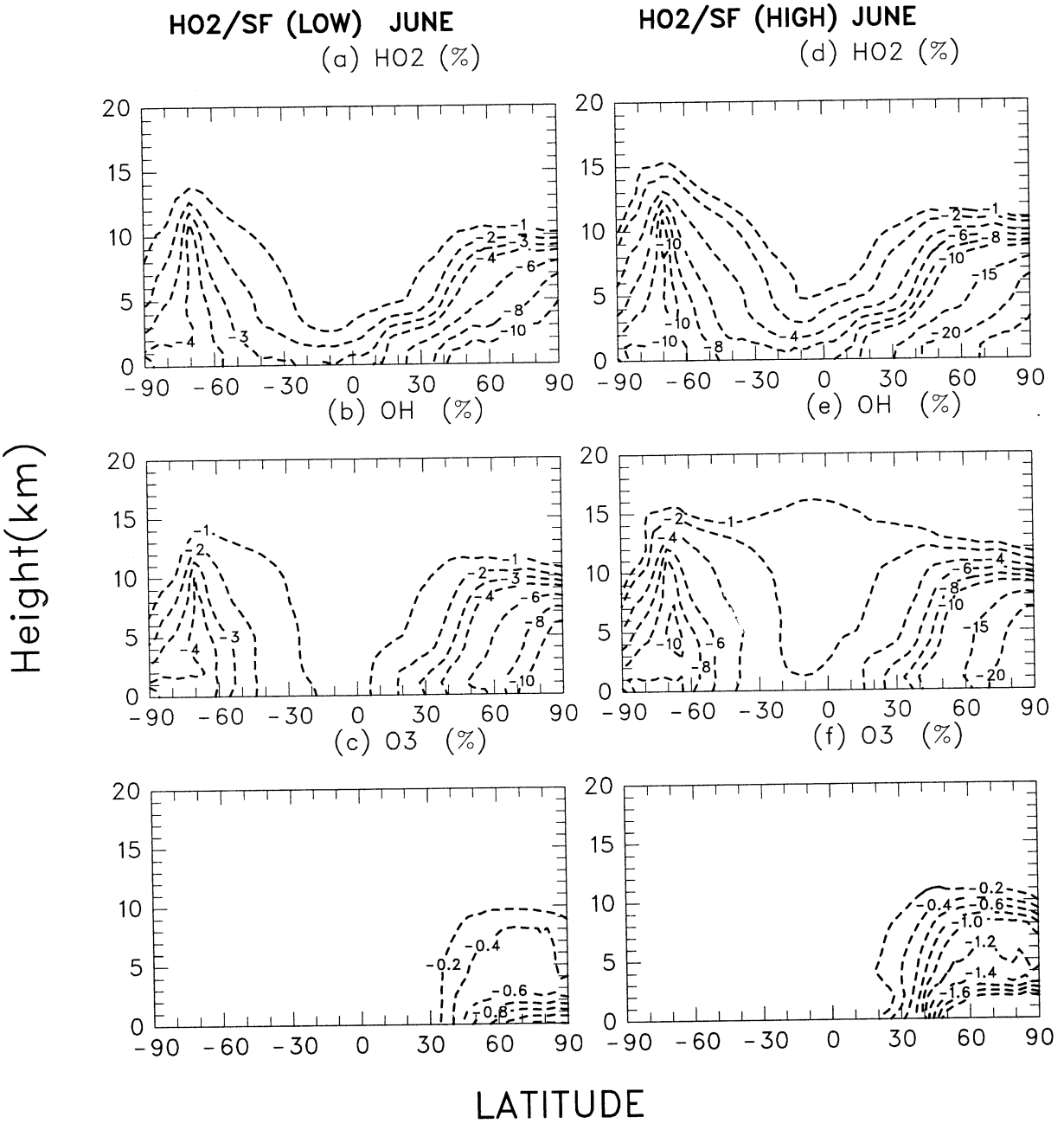

Figure 12. Changes (percent) due to the heterogeneous chemical reaction of HO_2 on (top) sulfate aerosols in HO_2, (middle) OH, and (bottom) O_3 with (left) $\gamma = 0.2$ and with (right) $\gamma = 0.5$ in June.

photochemical lifetime of OH. In contrast, the lifetime for HO_2 associated with gas-phase processes is longer than that of OH in the lower troposphere, so that heterogeneous uptake by sulfate aerosol can be comparable to photochemical destruction. Figure 11 shows that the photochemical lifetime of HO_2 is between 100 and 1000 s, while the time constant associated with heterogeneous uptake by sulfate aerosols is about 500 to 5000 s in the lower troposphere (Northern Hemisphere) during summer. Above 10 km, however, heterogeneous destruction is much slower than photochemical gas-phase destruction, and hence the presence of sulfate aerosols should not significantly affect HO_2 in the upper troposphere. During winter in the Antarctic the density of HO_2 is so small that the heterogeneous reaction does not play an important role in this region.

Figure 12 (top) shows the calculated changes (percent) in HO_2 due to uptake by sulfate aerosols (with uptake coefficients of 0.2 in left panels and 0.5 in right panels) in June. It indicates that HO_2 is reduced in the lower troposphere. The highest decrease (> 10%) occurs in northern mid- and high latitudes. The chemical lifetime (minutes) of HO_2 at these latitudes during summer is much smaller than the time constants associated with horizontal mixing and deposition. For steady-state conditions, the mass conservation of HO_2 can be expressed by

$$P = L = X/\tau, \tag{3}$$

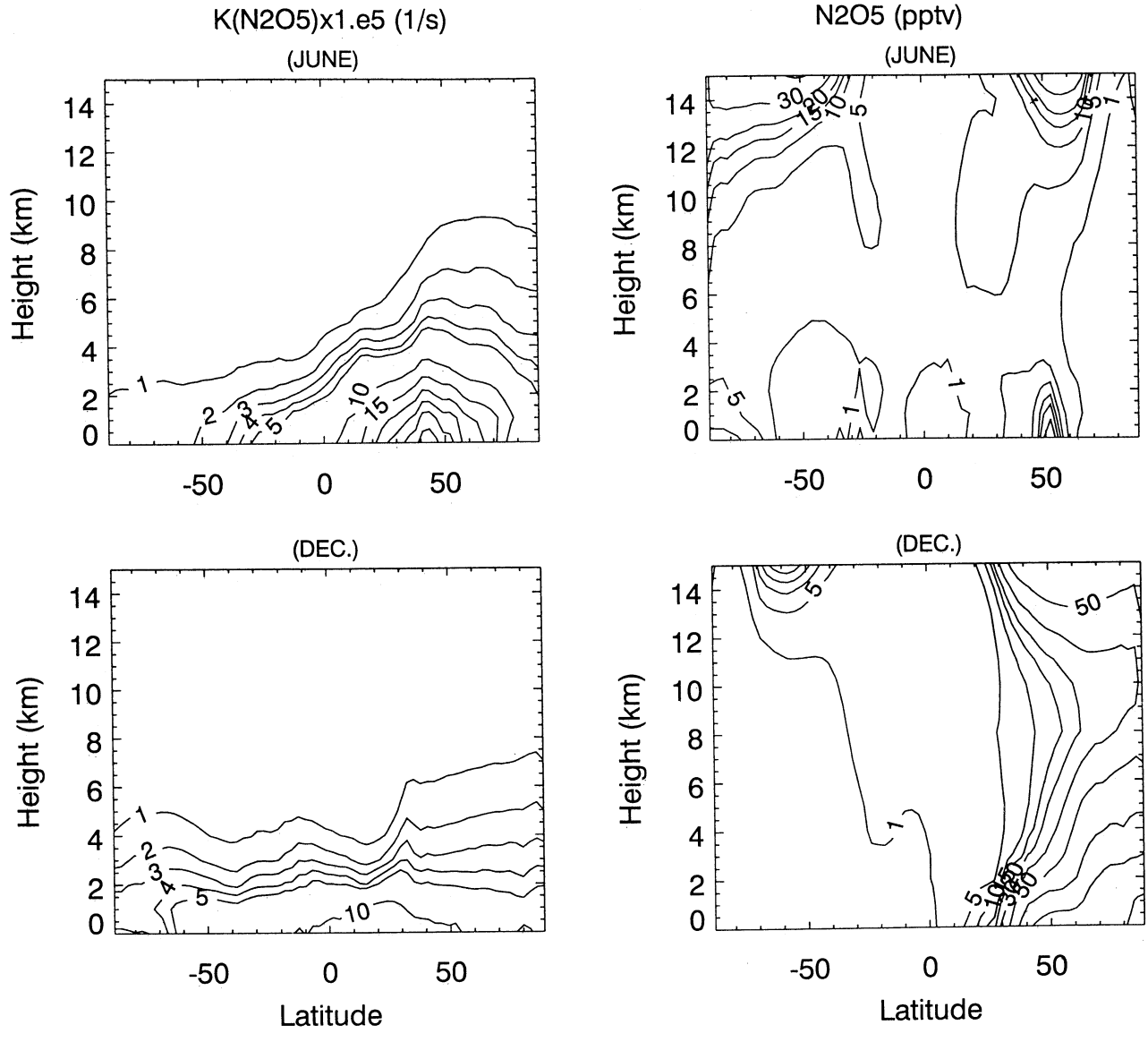

Figure 13. Zonally averaged reaction coefficient for N_2O_5 on sulfate aerosols (1/s) in (left) June and December, and zonally-averaged N_2O_5 mixing ratio (pptv) in (right) June and December.

where X is the mixing ratio of HO_2, P is its chemical production rate, L is its chemical loss rate, and τ is its chemical lifetime. The percentage change in the modeled HO_2 mixing ratio due to the addition of heterogeneous uptake is given by changes in its chemical lifetime can be estimated from (3):

$$\frac{\Delta X}{X} = -\frac{\tau_g}{\tau_g + \tau_h} \times 100\%, \quad (4)$$

where τ_g and τ_h are the photochemical and heterogeneous chemical lifetimes of HO_2, respectively. For example, for τ_g and τ_h equal to 500 and 5000 seconds respectively at 4 km at 80°N latitude, the estimated change in HO_2 is about −10% which is close to the model results shown in Figure 12.

Figure 12 (left) (with a lower uptake coefficient of 0.2) show that the changes in HO_2 lead to changes in OH and O_3 concentrations in the lower troposphere of the Northern Hemisphere during summer. Because HO_2 rapidly reacts with NO to produce OH and NO_2, the amount of HO_2 converted to OH is reduced when HO_2 is taken up by sulfate aerosols. The pattern of the OH decrease is similar to that of HO_2, with the highest reduction (10%) occurring at high northern latitudes below 5 km altitude. As the rate of HO_2 + NO reaction is reduced, the photochemical production of tropospheric ozone is also reduced. However, this process is in competition with the HO_2 + O_3 reaction which destroys ozone. As a result the net change in O_3 concentration associated with heterogeneous uptake of HO_2 is very small (less than 1% reduction).

A high uptake coefficient is suggested by *Cantrell et al.* [1996]. According to their study, this uptake coefficient could be as high as 0.5 to 1.0. Figure 12 (right) shows the model results when the adopted uptake coefficient is 0.5. Compared to the results with uptake coefficient of 0.2, the decrease in HO_2 density calculated in this case is approximately twice as large with a 20%

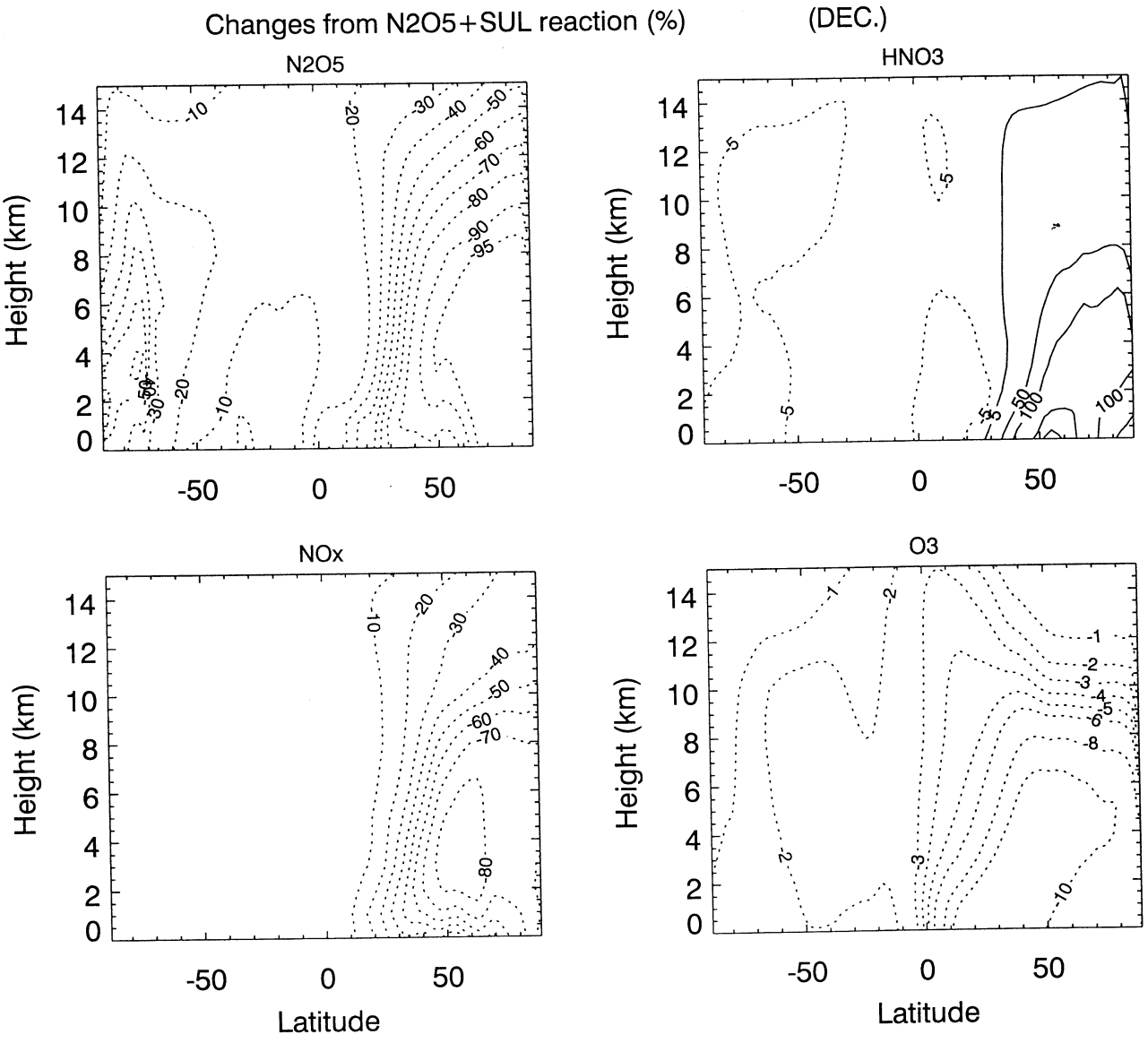

Figure 14. Calculated changes (percent) due to the heterogeneous chemical reaction of N_2O_5 on sulfate aerosols for (a) N_2O_5, (b) HNO_3, (c) NO_x, and (d) O_3 in December.

reduction in the lower troposphere of the northern hemisphere during summer. Since the heterogeneous chemical lifetime τ_h is inversely proportional to the uptake coefficient γ (see (1)), a 2.5 times increase in γ leads to a maximum of a 25% decrease in the HO_2 density. With an uptake coefficient reaching its upper limit of 1.0, the reduction in HO_2 predicted from (4) could be as large as 50% in the lower troposphere of the Northern Hemisphere during summer.

4.4. Reaction of N_2O_5 on Sulfate Aerosols

The reaction of N_2O_5 on the surface of sulfate aerosols (N_2O_5 + SF) plays an important role in the lower stratosphere, as highlighted by *Hofmann and Solomon* [1989], *Brasseur et al.* [1990], *Rodriguez et al.* [1991], *Fahey et al.* [1993], and *Tie et al.* [1994b]. These studies show that this process is efficient in converting N_2O_5 into HNO_3 during wintertime at middle to high latitudes. Because N_2O_5 is formed by the reaction of NO_2 + NO_3, NO_x concentrations are also significantly reduced by this mechanism. The study by *Tie et al.* [1994b] suggests that NO_2 was reduced by as much as a factor of 2 at midlatitudes in the lower stratosphere after the volcanic eruption of Mount Pinatubo in 1991. However, the effects of this reaction in the troposphere have not yet been completely assessed.

According to the (R13) and (1), the heterogeneous conversion of N_2O_5 to HNO_3 depends strongly on the first-order rate coefficient for the heterogeneous reaction and the concentration of gas-phase N_2O_5. Figure 13 shows the zonal mean rate coefficient for heterogeneous reaction (R13) and the N_2O_5 mixing ratio in June and December. The highest reaction coefficients are found with a maximum of 40 x 10^{-5} (1/s), corresponding to a lifetime of N_2O_5 of ~ 40 min in northern midlatitudes in June. During northern hemispheric winter (December) the maximum of the reaction rate is reduced to 10 x 10^{-5} (1/s), corresponding to a lifetime for N_2O_5 of ~3 hours, because of the smaller loading of

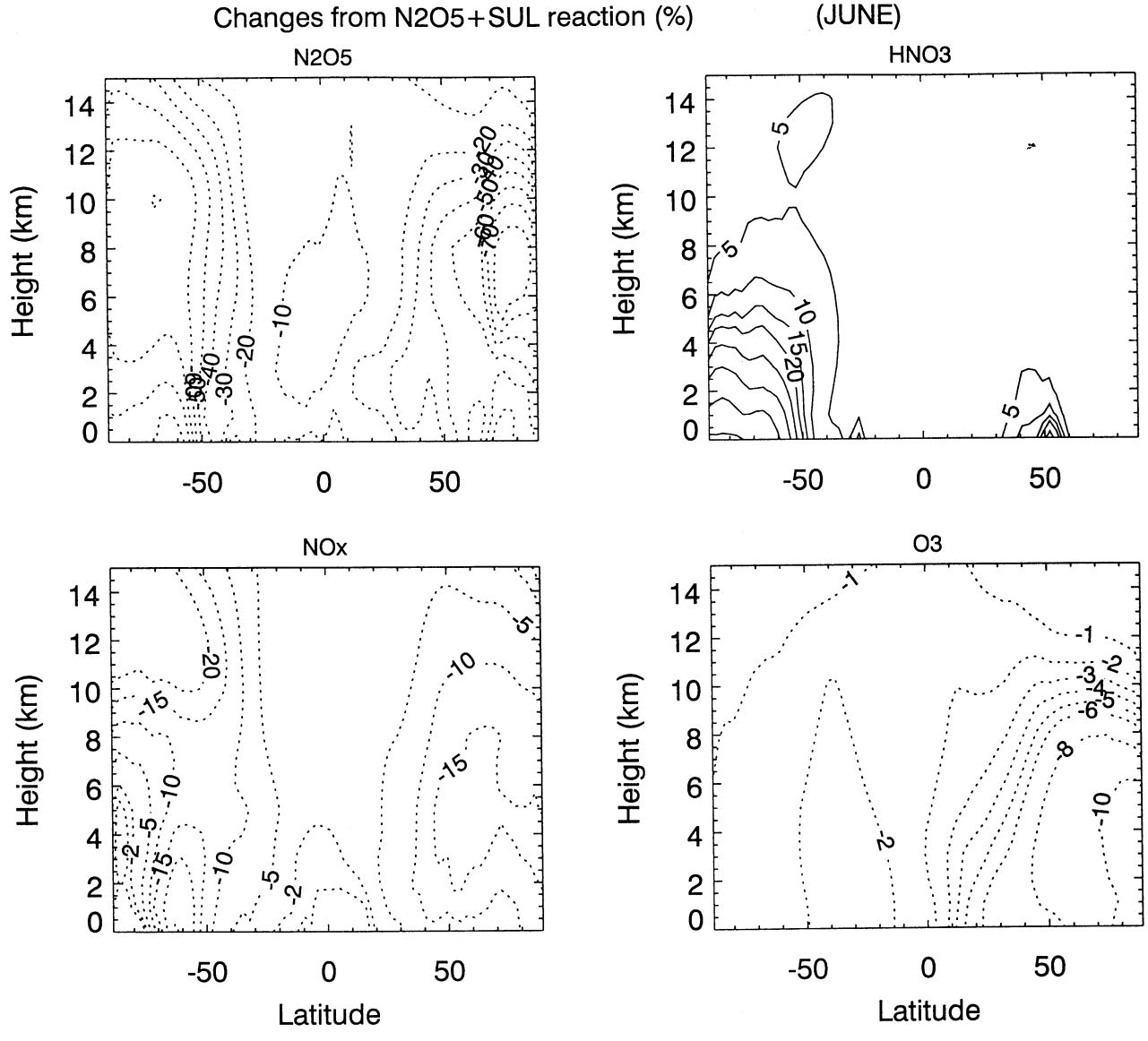

Figure 15. Same as Figure 14, but in June.

sulfate aerosols (see Figure 4). The concentration of N_2O_5 has a maximum in midlatitudes in the boundary layer in the same location as the elevated sulfate aerosols from anthropogenic emissions. However, the strong temperature dependent thermal decomposition of N_2O_5 in the boundary layer produces a strong seasonal variability of N_2O_5 in the boundary layer of the middle latitudes of the Northern Hemisphere where large sulfate aerosol loading is located. During summer the concentration of N_2O_5 in the region is generally ~ 1 pptv, while in the winter it is ~ 50 to 100 pptv.

Without the heterogeneous conversion of N_2O_5 into nitric acid, N_2O_5 is mainly formed and destroyed by the following reactions:

(R16) $NO_2 + O_3 \rightarrow NO_3 + O_3$,

(R17) $NO_3 + NO_2 + M \rightarrow N_2O_5 + M$,

(R18) $N_2O_5 + M \rightarrow NO_2 + NO_3 + M$.

The rate-limiting step provided by the rate of (R16). The reactions (R17) and (R18) are cycling reactions between NO_2, NO_3, and N_2O_5. The heterogeneous reaction (R13) provides a chemical destruction for N_2O_5 and NO_x as well as a chemical production for HNO_3. The rate of (R13) is dependent upon the reaction coefficient of (R13) and the background concentration of N_2O_5 shown in Figure 13. During winter the background concentration of N_2O_5 is much higher than during summer, and a large decrease in the N_2O_5 and NO_x concentrations is expected. Figure 14 shows that in northern middle to high latitudes, the heterogeneous conversion of N_2O_5 to HNO_3 plays a very important role during winter. In December the decrease in northern hemispheric N_2O_5 is ~ 95%, and the decreases in NO_x is ~ 70 to 80% in the Northern Hemisphere, while, in June, the decrease in N_2O_5 is ~ 50 to 70%, and in NO_x is ~ 10 to 15% (see Figure 15). Since tropospheric ozone is produced by the oxidation of hydrocarbons and CO catalyzed by hydrogen oxide radicals (HO_x = OH + HO_2) and nitrogen oxide radicals (NO_x = NO + NO_2), changes in NO_x in the troposphere lead to changes in the production of O_3. At midlatitudes in the Northern Hemisphere the decrease in NO_x (10 to 15% reduction) in June produces an 8 to 10% ozone reduction

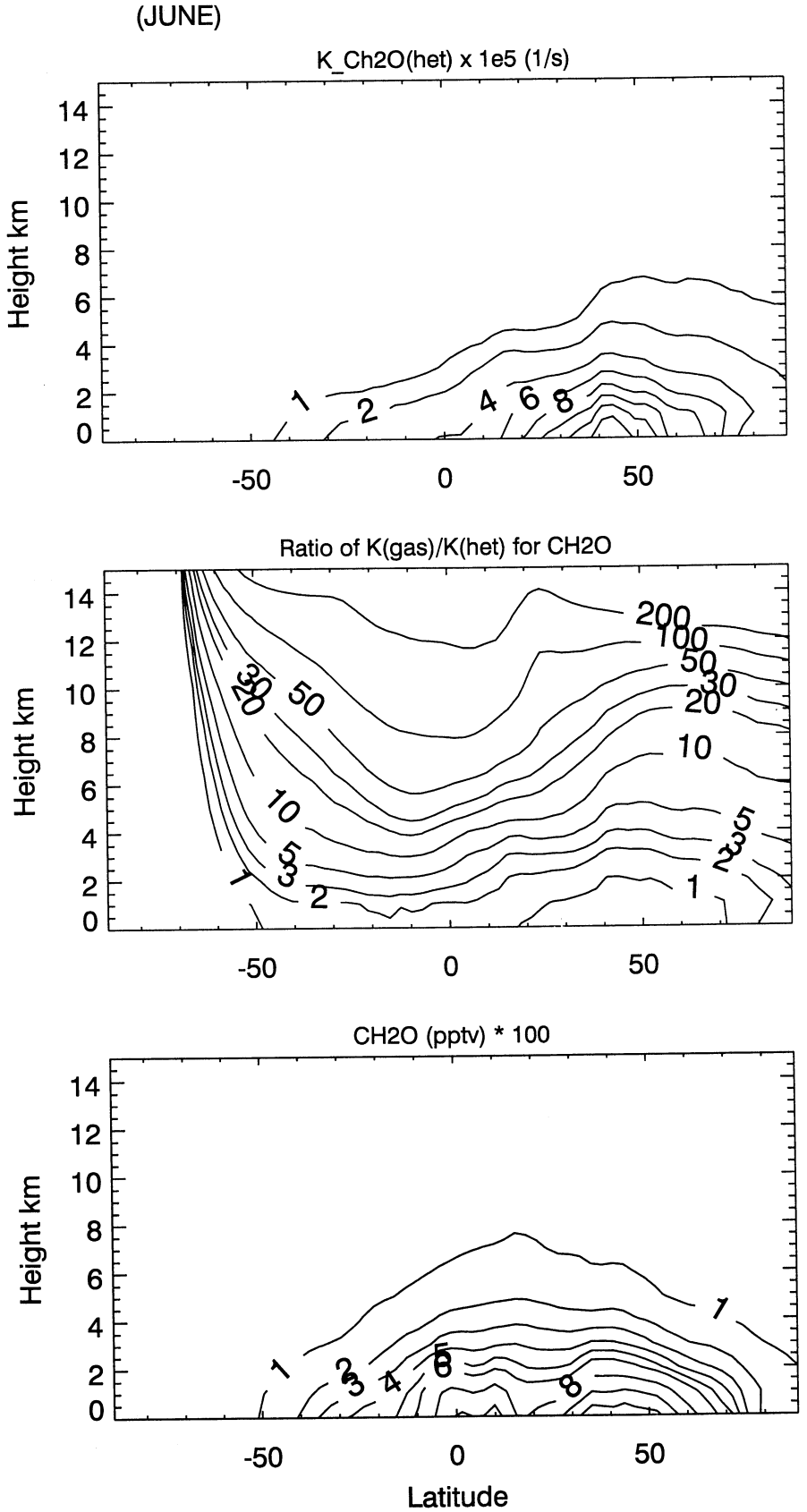

Figure 16. (top) Zonally-averaged reaction coefficient for CH_2O on sulfate aerosols (1/s), the ratio of the gas-phase reactions (R19), (R20), and (R21) to the (middle) heterogeneous reaction (R13), and (bottom) CH_2O mixing ratio (pptv) in June.

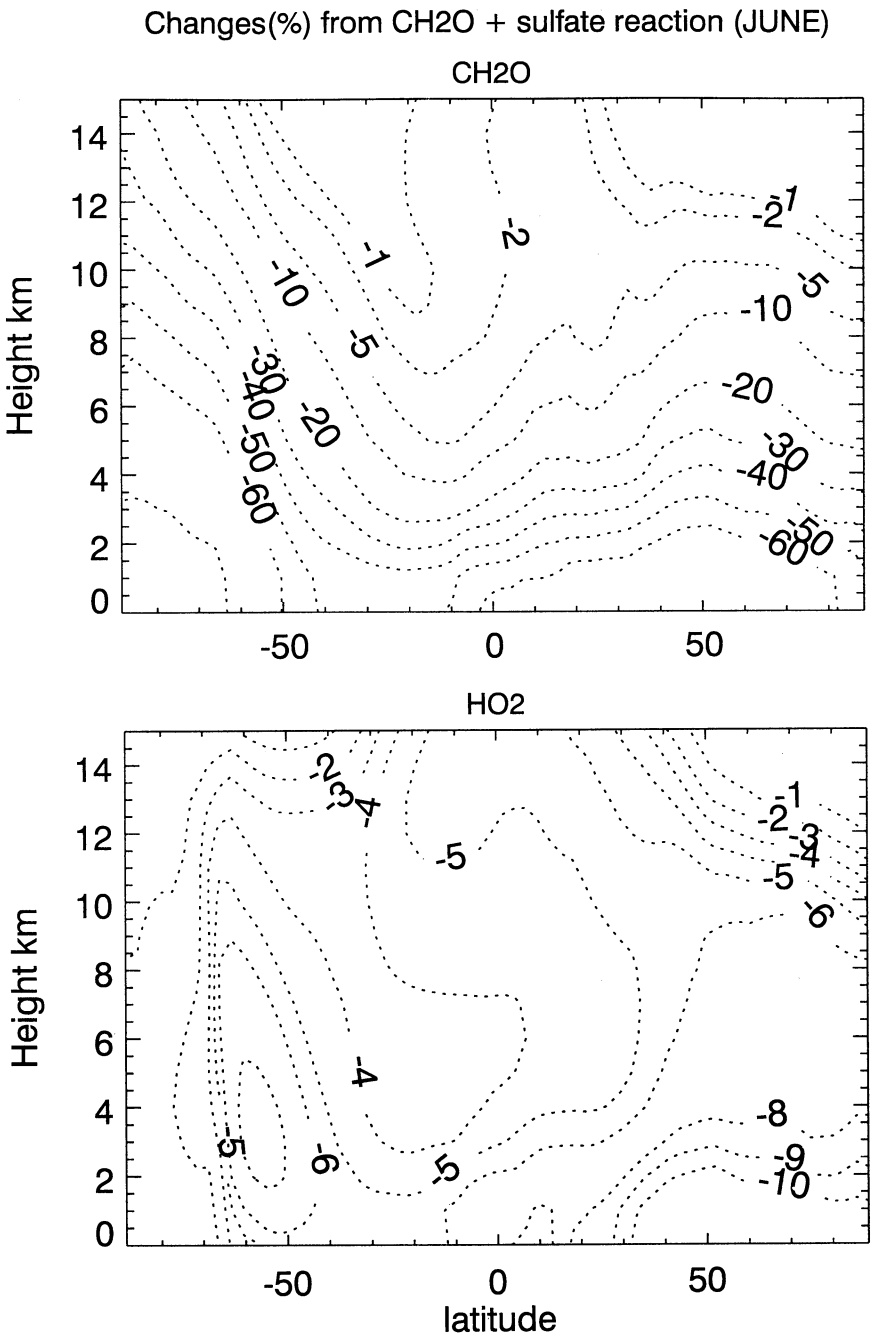

Figure 17. Calculated changes (percent) due to the hetero-geneous chemical reaction of CH_2O with uptake coefficient of $\gamma = 0.022$ on sulfate aerosols for (top) CH_2O and (bottom) HO_2 in June.

(see Figure 15). However, in December, although a large decrease in NO_x is calculated (70 to 80%), the change in O_3 is ~ 10% because the oxidation of hydrocarbons and CO is small (see Figure 14). The calculation by *Dentener and Crutzen* [1993] suggests a very large decrease (80%) in NO_x in the lower troposphere during winter due to this heterogeneous process, which is consistent with our calculation, but the change in O_3 (25% decrease) is some what larger than our calculation.

4.5. Reaction of CH_2O on Sulfate Aerosols

Photolysis of formaldehyde (CH_2O) provides a source of HO_x radicals. Field measurements show that CH_2O concentrations calculated from gas-phase models have a tendency to overestimate the observed CH_2O at Mauna Loa, Hawaii [*Liu et al.*, 1992]. Reaction of CH_2O in sulfate aerosols has been proposed as a possible explanation [*Chatfield*, 1994]. The MOZART calculation of CH_2O without the reaction of CH_2O on sulfate aerosols tends to overestimate the observed concentrations of CH_2O in the continental boundary layer during summer [*Hauglustaine et al.*, 1998]. The uptake of gas-phase CH_2O by sulfate aerosol particles has been measured as a function of temperature and acid concentration by *Jayne et al.* [1996]. Their measurements show that the uptake coefficient of CH_2O on sulfate aerosols varies from 0.01 to 0.022 according to acid concentrations and temperatures. These uptake coefficients should

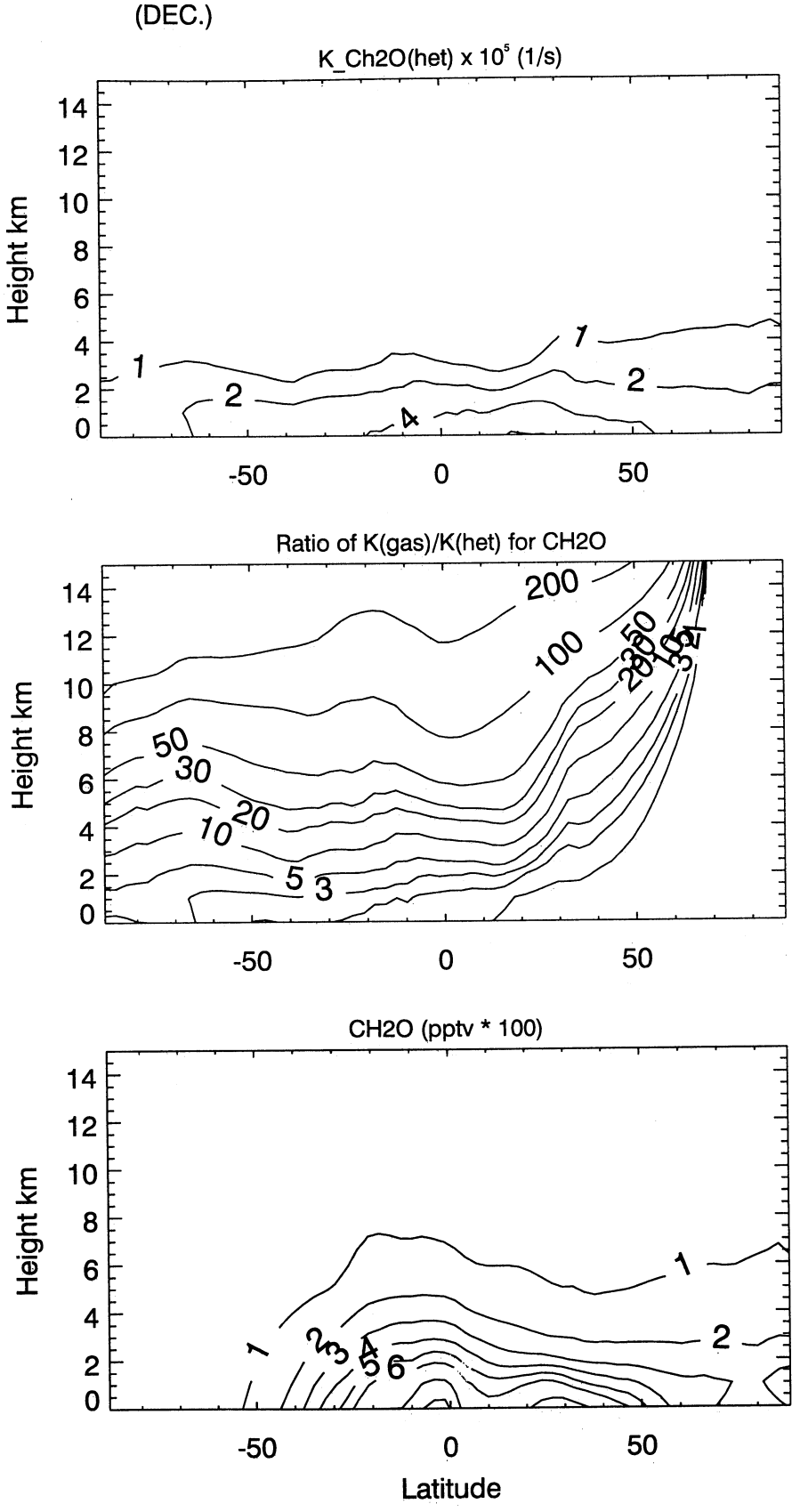

Figure 18. Same as Figure 17, but in December.

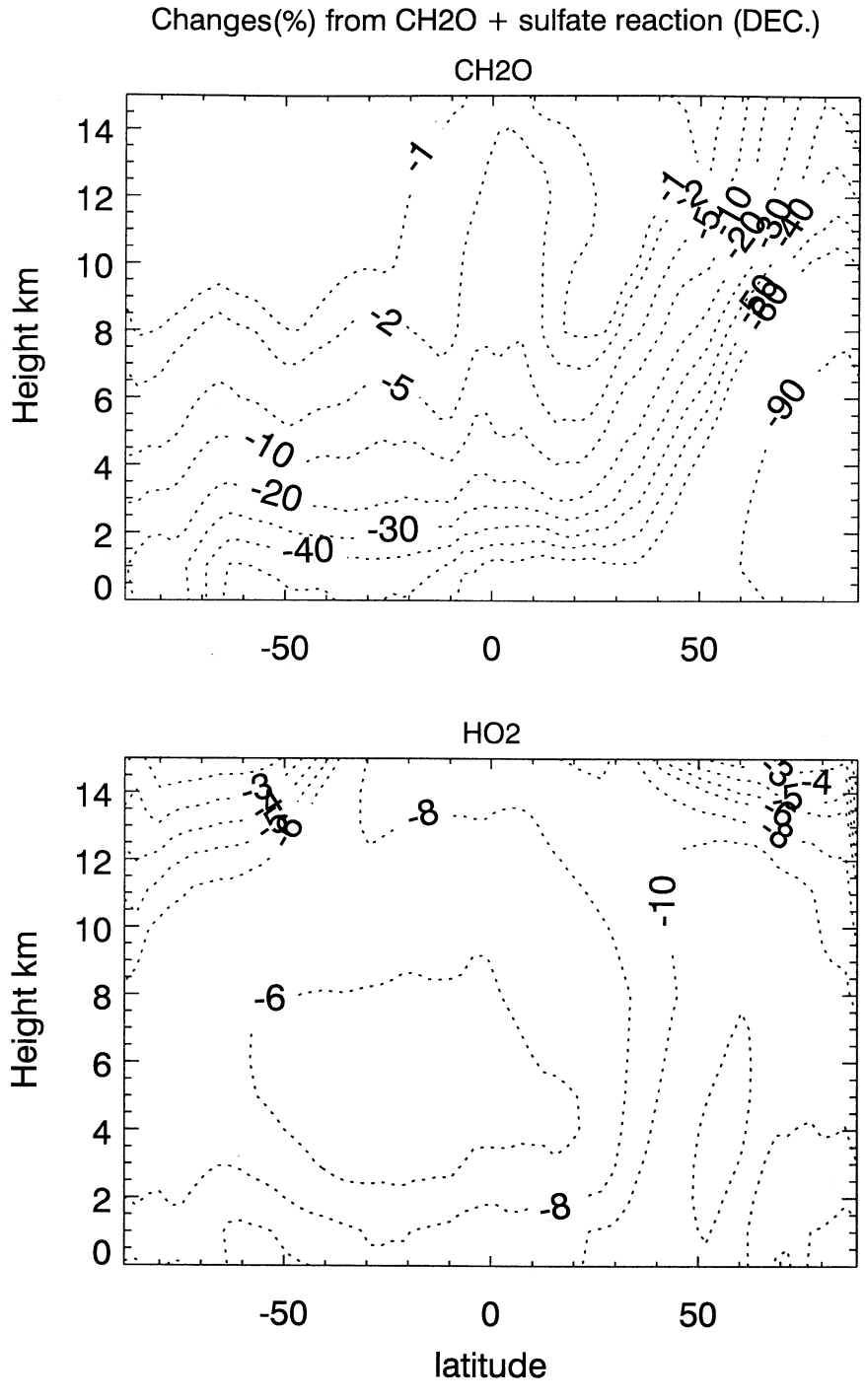

Figure 19. Same as Figure 17, but in December.

be regarded as solubility-determined upper limits, so that the calculated reduction in the CH_2O concentration should be considered as upper limits.

Without the heterogeneous uptake of CH_2O on sulfate aerosols, CH_2O would be destroyed by

(R19) $CH_2O + h\nu \rightarrow CO + H_2$,

(R20) $CH_2O + h\nu \rightarrow CO + 2HO_2$,

(R21) $CH_2O + OH \rightarrow CO + HO_2 + H_2O$.

Reaction (R20) leads to the production of HO_x. With the heterogeneous uptake of CH_2O into sulfate aerosols, the HO_x concentrations are reduced. Figure 16 shows that the rate of heterogeneous reaction of CH_2O is highest (with a uptake coefficient of 0.022) at northern midlatitudes in the boundary layer in June, where the ratio of the rate of the gas-phase reactions (R19), (R20), and (R21) to the rate of the heterogeneous reaction (R14) is significantly less than one, and hence heterogeneous reaction (R14) plays a very important role in this region. As a result, the concentration of CH_2O is reduced by 60% and HO_2 is reduced by 10% in this region in June (see Figure 17). Furthermore the effect of (R14) on CH_2O and HO_x has a very strong seasonal variation. As indicated in Figure 18, in December, the rate of heterogeneous reaction of CH_2O decreases due to the

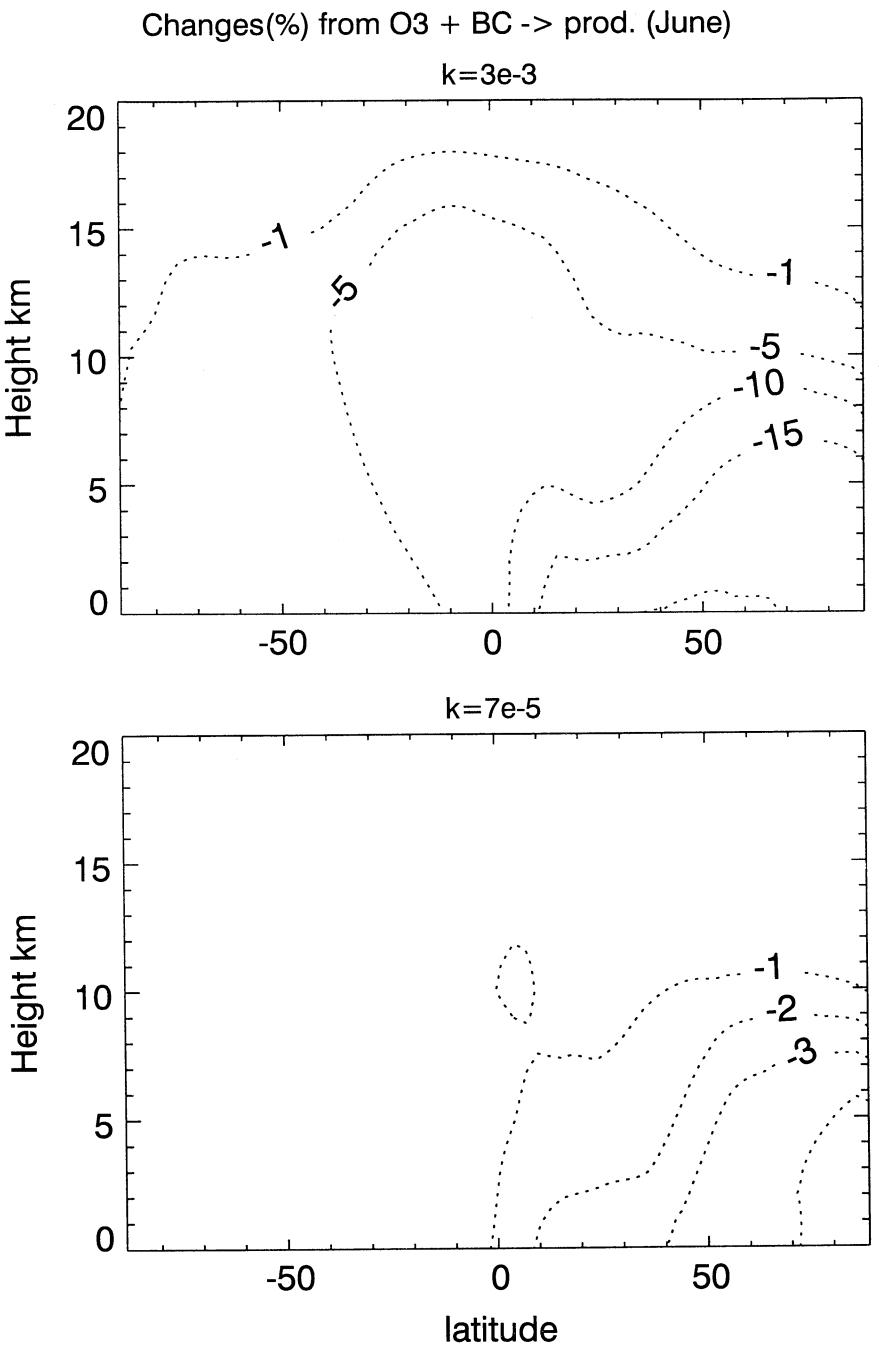

Figure 20. Calculated changes in O_3 (percent) due to the heterogeneous chemical reaction of O_3 on soot with (top) uptake coefficient of $3x10^{-3}$ and (bottom) uptake coefficient of $7x10^{-5}$ in June.

smaller sulfate aerosol loading in northern midlatitudes in the boundary layer. However, the rates of the gas-phase photochemical reactions (R19), (R20), and (R21) are also significantly reduced during winter in this region. As a result, the heterogeneous reaction (R14) plays a very important role in the Northern Hemisphere during winter, producing a 90% decrease in CH_2O and a 10% decrease in HO_2 in northern middle and high latitudes (see Figure 19). With a lower uptake coefficient for CH_2O (γ = 0.011), the changes in CH_2O and HO_2 are slightly reduced, but the impact of (R14) remains important with reductions in CH_2O and HO_2 of 50 and 8% in northern midlatitudes in the boundary layer during June.

4.6. Reaction of O_3 on Black Carbon

The effects of O_3 uptake by black carbon particles on the tropospheric ozone budget have not yet been addressed by global chemical models. On the basis of laboratory studies, *Fendel et al.* [1995] and *Rogaski et al.* [1997] have shown that the uptake coefficient for ozone on black carbon particles occurs with an uptake coefficient of the order of $2x10^{-4}$ to $3.3x10^{-3}$. On the other hand, *Saathoff* [1999] shows the reaction coefficient is only on the order of $7x10^{-5}$. The reason for the smaller reaction coefficients is that their measurements were made over a longer timescale than in the previous studies, and thus the sites on the surface of soot

Table 5. Summary of the Effects of Heterogeneous Reactions on Chemical Oxidants Calculated by the Model at 5 km in June[a]

Reactions		Changes, %		
		45°N	Equator	45°S
	June			
(1) N_2O_5 +sulfate	NO_x	-7	-2	-2
($\gamma = 0.1$)	HNO_3	8	0	-17
	O_3	-7	-2	-2
(2) HO_2 + sulfate	HO_2	-10	-1	-6
($\gamma = 0.5$)	OH	-11	-2	-7
	O_3	-3	-1	-1
(3) CH_2O + sulfate				
($\gamma = 0.011$)	CH_2O	-31	-8	-25
	HO_2	-7	-3	-6
	December			
(1) N_2O_5 +sulfate	NO_x	-73	-3	-6
($\gamma = 0.1$)	HNO_3	30	-4	-4
	O_3	-11	-3	-2
(2) HO_2 + sulfate	HO_2	-9	0	-1
($\gamma = 0.5$)	OH	-16	-5	-7
	O_3	0	0	-2
(3) CH_2O + sulfate				
($\gamma = 0.011$)	CH_2O	-6	-9	-46
	HO_2	-6	-5	-12

[a]The values represent the zonally averaged changes (percent) in the indicated oxidant when heterogeneous reactions are included with the gas-phase chemistry only.

are deactivated as suggested by *Aumount et al.* [1999]. The uptake coefficient for O_3 on soot particles is relatively low compared to the uptake coefficient of HO_2 and N_2O_5 on sulfate aerosols, and compared to the uptake of HNO_3 on soot reactions. However, since the destruction of O_3 due to gas-phase reactions in the lower troposphere is relatively slow (weeks to months) [*Liu*, 1988], the heterogeneous reaction of O_3 on soot could potentially enhance the destruction of O_3 in the lower troposphere. We have used the uptake coefficient of 3.3×10^{-3} for a upper limit value and 7×10^{-5} for a lower limit value for the reaction of O_3 on soot in the model. Only hydrophobic soot surface area will be used for this reaction. Once the soot surface is coated by other aerosols, the reaction will not take place.

Figure 20 shows the impact of this reaction on O_3 concentrations. If the high value of the uptake coefficient ($\gamma = 3 \times 10^{-3}$) is adopted, the O_3 destruction rate at midlatitudes and high latitudes of the Northern Hemisphere is dominated by the heterogeneous reaction with black carbon, producing very large O_3 destruction in the lower troposphere. The maximum reduction in O_3 concentration reaches 15% in June (see Figure 20 (top)). However, with the low value of the uptake coefficient ($\gamma = 7 \times 10^{-5}$), the decrease in the O_3 concentration is modest. The maximum O_3 reduction is 3 to 4% in midlatitudes to high latitudes of the Northern Hemisphere (see Figure 20 (bottom)). Because this calculation suggests that the effect of the soot surface reaction on O_3 depends strongly upon the uptake coefficient, further laboratory measurements for this reaction are needed.

5. Summary

A global interactive chemical and aerosol model has been developed to study the distribution of sulfate and soot aerosol particles and their effects on tropospheric oxidants. The simulated global sulfate aerosol distributions and seasonal variation have been compared with observations. The seasonal variation of sulfate aerosols is in agreement with measurements, except in the Arctic region. The calculated vertical profiles of sulfate aerosols agree with the observations over North America. In the case of black carbon, the calculated surface distribution is in fair agreement with observations. We have conducted the following studies to calculate the potential effects of aerosols on atmospheric chemical constituents; (1) the impact on the oxidant level of the chemical conversion of SO_2 to $SO_4^=$; (2) the effects of N_2O_5, HO_2, and CH_2O reactions reactions on chemical composition taking place on sulfate aerosols. The effect of heterogeneous reactions on tropospheric oxidants at different regions is briefly summarized in Table 5. The results indicate that with an uptake coefficient of 0.5, the heterogeneous reaction of HO_2 on the surface of sulfate aerosols produces a significant loss of HO_2 and OH. The largest reduction in the OH abundance occurs at high northern latitudes in the lower troposphere, with a 10% decrease during summer and a 15% decrease during winter. However, this result should be regarded as an upper limit estimation. The N_2O_5 reaction on the surface of sulfate aerosols produces a 80% reduction of NO_x at midlatitudes to high latitudes during winter. Because ozone production efficiency is low in winter, this decrease in NO_x leads to less than 10 percent decrease in ozone in the model. The heterogeneous reaction of CH_2O on sulfate aerosols produces a significant decrease in the concentrations of CH_2O and HO_2. Further laboratory measurements of the reaction coefficients are needed to reduce the uncertainties on the calculated effects of heterogeneous reactions on tropospheric oxidants.

Acknowledgments. The authors are grateful to John Orlando and William Collins for useful comments on the manuscript. The work of X. Tie and Guy Brasseur is partially supported by DOE Atmospheric Chemistry Program under contract DE-AI05-98ER62579. Louisa Emmons is supported by NASA under interagency-agreement L-9301. The National Center for Atmospheric Research is operated by the University Corporation for Atmospheric Research under the sponsorship of the National Science Foundation.

References

Andreae, M. O., and P.J. Crutzen, Atmospheric aerosols: biogeochemical sources and role in atmospheric chemistry, *Science, 276*, 1052-1058, 1997.

Andreae, M.O., T.W. Andreae, R.J. Ferek, and H. Raemdonck, Long range transport of soot carbon in the marine atmosphere, *Sci. Total Environ., 36*, 73-80, 1984.

Aumont, B., S. Madronich, M. Ammann, M. Kalberer, U. Baltensperger, D. Hauglustaine, and F. Brocheton, On the NO_2 + soot reaction in the atmosphere, *J. Geophys. Res., 104*, 1729-1736, 1999.

Atkinson R., D.L. Baulch, R.A. Cox, R.F. Hampson, J.A. Kerr, and J. Troe, Evaluated kinetic and photochemical data for atmospheric chemistry: Supplement IV, *Atmos. Environ., Part A, 26*, 1187-1230, 1992.

Barth, M.C., P.J. Rasch, J.T.Kiehl, C.M. Benkovitz, and S.E. Schwartz, Sulfur chemistry in the NCAR CCM: Description, evaluation, features and sensitivity to aqueous chemistry, *J. Geophys. Res., 105*, 1387-1415, 2000.

Benkovitz, C.M., C.M. Berkowitz, R.C. Easter, S. Nemesure, R. Wagener, S. E. Schwartz, Sulfate over the North Atlantic and adjacent continental regions: Evaluation for October and November 1986 using a three-dimensional model driven by observation-derived meteorology, *J. Geophys. Res., 99*, 20,725-20,756, 1994.

Benkovitz, C.M., M.T. Scholtz, J. Pacyna, L. Tarrason, J. Diagnon, E.C. Voldner, P.A. Spiro, J.A. Logan, and T.E. Graedel, Global gridded inventories of anthropogenic emissions of sulfur and nitrogen, *J. Geophys. Res., 101*, 29,239-29,253, 1996.

Blake, D.F., and K. Kato, Latitudinal distribution of black carbon soot in

the upper troposphere and lower stratosphere, *J. Geophys. Res., 100,* 7195-7202, 1995.

Bond, T.C., R.J. Charlson, and J. Heintzenberg, Quantifying the emission of light-absorbing particles: Measurements tailored to climate studies, *Geophys. Res. Lett., 25,* 337-340, 1998.

Brasseur, G. P., D. A. Hauglustaine, S. Walters, J. F. Müller, P. Rasch, C. Granier, and X. Tie, MOZART: A global chemical transport model for ozone and related chemical tracers, 2. Model results and evaluations, 1, Model description, *J. Geophys. Res., 103,* 28,265-28,289, 1998.

Brasseur, G. P., C. Granier, and S. Walters, Future changes in stratospheric ozone and the role of heterogeneous chemistry, *Nature, 348,* 626-628, 1990.

Cantrell, C.A., R.E. Shetter, T.M. Gilpin, J.G. Calvert, F.L. Eisele, and D.J. Tanner, Peroxy radical concentrations measured and calculated from trace gas measurements in the Mauna Loa Observatory Photochemistry Experiment 2, *J Geophys. Res., 101,* 14,653-14,664, 1996.

Charlson, R.J., J. Langner, H. Rodhe, C.B. Leovy, and S.G. Warren, Perturbation of the northern hemisphere radiative balance by backscattering from anthropogenic sulfate aerosols, *Tellus, Ser. B, 43*(4), 152-163, 1991.

Chatfield, R.B., Anomalous HNO_3/NO_x ratio of the remote tropospheric air: Conversion of nitric acid to formic acid and NO_x? *Geophys. Res. Lett., 21,* 2705-2708, 1994.

Chin, M., D. Jacob, G. Gardner, F. Foreman, S. Michael, A. Peter, L. Dennis, A global three- dimensional model of tropospheric sulfate, *J. Geophys. Res., 101,* 18,667-18,690, 1996.

Choi, W., and M. T. Leu, Nitric acid uptake and decomposition on black carbon (soot) surface: Its implications for the upper troposphere and lower stratosphere, *J. Phys. Chem. A, 102,* 7618-7630, 1998.

Cooke, W.F., and J.J.N. Wilson, A global black carbon aerosol model, *J Geophys. Res., 101,* 19,395-19,409, 1996.

Crutzen, P.J., The possible importance of OCS for the sulfate layer of the stratosphere, *Geophys. Res. Lett., 3,* 73-76, 1976.

DeMore, W.B, et al., Chemical kinetics and photochemical data for use in stratospheric modeling, *JPL Publ. 97-4,* Jet Propul. Lab., Pasadena, Calif., 1997.

Dentener, F.J., and P.J. Crutzen, Reaction of N_2O_5 on tropospheric aerosols: Impact on the global distributions of NO_x, O_3, and OH, *J. Geophys. Res., 98,* 7149-7163, 1993.

Dentener, F.J., and P.J. Crutzen, A three-dimensional model of the global ammonia cycle, *J. Atmos. Chem. 19,* 331-369, 1994.

Dentener, F.J., and P.J. Crutzen, Role of mineral aerosol as a reactive surface in the global troposphere, *J. Geophys. Res., 101,* 22,869-22,889, 1996.

Dentener, F. J., C. R. Carmichael, Gregory, Y. Zhang, L. Yang, J. Lelieveld, and P. J. Crutzen, Role of mineral aerosol as a reactive surface in the global troposphere, *J. Geophys. Res., 98,* 22,869-22,889, 1996.

Fahey, D. W., et al., In situ measurements constraining the role of sulfate aerosols in mid-latitude ozone depletion, *Nature, 363,* 509-514, 1993.

Feichter, J., E. Kjellstrom, H. Rodhe, F. Dentener, J. Lelieveld, and G.-J. Roelofs, Simulation of the tropospheric sulfur cycle in a global climate model, *Atmos. Environ., 30,* 1693-1707, 1996.

Fendel, W., and A. S. Ott, Ozone depletion potential of carbon aerosol particles, *J. Aerosol Sci., 24,* 317-318, 1993.

Fendel, W., D. Matter, H. Burtscher, and A. Schmidt-Ott, Interaction between carbon or iron aerosol particles and ozone, *Atmos. Envrion., 29,* 967-973, 1995.

Ferek, R.J., J.S. Reid, and P.V. Hobbs, Emission factors of hydrocarbons, halocarbons, trace gases and particles from biomass burning in Brazil, *J. Geophys. Res., 103,* 32,107-32,118, 1988.

Fried, A., B. E. Henry, J.G. Calvert, and M. Mozurkewich, The reaction probability of N_2O_5 with sulfuric acid aerosols at stratospheric temperatures and compositions, *J. Geophys. Res., 99,* 3517-3532, 1994.

George, Ch., J. L. Ponche, Ph. Mirabel, W. Behnke, V. Scheer, and C. Zetsch, Study of the uptake of N_2O_5 by water and NaCl solutions, *J. Phys. Chem., 98,* 8780-8784, 1994.

Giorgi, F., and W.L. Chameides, The rainout parameterization in a photochemical model, *J. Geophys. Res., 90,* 7872-7880, 1985.

Golden, D.M., and J. Manion, Applications of chemical kinetics, *Adv. Chem. Kinet. Dyn., 1,* 187-276, 1992.

Goodman, A.L., G.M. Underwood, and V.H. Grassian, Heterogeneous reaction of NO_2: Characterization of gas-phase and adsorbed products from the reaction, $2NO_2(g) + H_2O(a) \rightarrow HONO(g) + HNO_3(a)$ on hydrated silica particles, *J. Phys. Chem. A, 103,* 7217-7223, 1999.

Hack, J. J., B. A. Boville, B. P. Briegleb, J. T. Kiehl, P. J. Rasch, and D. L. Williamson, Description of the NCAR community climate model (CCm^2), *Tech. Note NCAR/TN- 382+STR,* 108 pp., Natl. Cent. for Atmos. Res., Boulder, Colo., 1993.

Hagen, D.E., M.B. Trueblood, and P.D. Whitefield, A field sampling of jet exhaust aerosols, *Particulate Sci. Tech., 10,* 53-63, 1992.

Hanson, D. H., and E.R. Lovejoy, The uptake of N_2O_5 onto small sulfuric acid particles, *Geophys. Res., Lett., 21,* 2401-2404, 1994.

Hanson, D. H., and A. R. Ravishankara, The reaction probability of $ClONO_2$ and N_2O_5 on 40 to 75% sulfuric acid solutions, *J. Geophys. Res., 96,* 17,307-17,314, 1991.

Hanson, D. H., and A. R. Ravishankara, Investigation of the reactive and nonreactive processes involving $ClONO_2$ and HCl on water and nitric acid doped ice, *J. Phys. Chem., 96,* 2682- 2691, 1992.

Hauglustaine, D. A., B.A. Ridley, S. Solomon, P.G. Hess, and S. Madronich, HNO_3/NO_x ratio in the remote troposphere during MLOPEX 2: Evidence for nitric acid reduction on carbonaceous aerosols? *Geophys. Res. Lett., 23,* 2609-2612, 1996.

Hauglustaine, D. A., G.P. Brasseur, S. Walters, P.J. Rasch, J.F. Muller, L.K. Emmons, and M. A. Carroll, MOZART, A global chemical transport model for ozone and related chemical tracers, Model results and evaluations, *J. Geophys. Res., 103,* 28,291-28,335, 1998.

He, S., and G.R. Carmichael, Sensitivity of photolysis rates and ozone production in the troposphere to aerosol properties, *J. Geophys. Res., 104,* 26,307-26,324, 1999.

Holtslag, A. A. M., and B. A. Boville, Local versus nonlocal boundary-layer diffusion in a global climate model, *J. Clim., 6,* 1825-1842, 1993.

Hidy, G. M., Assessment of regional air pollution over the eastern United States: Results from the Sulfate Regional Experiment (SURE), *Rep. WMO 538,* pp. 65-76, World Meteorol. Org., Geneva, 1979.

Hofmann, D. J., and S. Solomon, Ozone destruction through heterogeneous chemistry following the eruption of El Chichón, *J. Geophys. Res., 94,* 5029-5041, 1989.

Hofmann, D. J., S. J. Oltmans, W. D. Komhyr, J. M. Harris, J. A. Lathrop, A. O. Langford, T. Deshler, B. J. Johnson, A. Torres, and W. A. Matthews, Ozone loss in the lower stratosphere over the United States in 1992-1993: Evidence for heterogeneous chemistry on the Pinatubo aerosol, *Geophys. Res. Lett., 21,* 65-68, 1994.

Hu, J.H., and J.P.D. Abbatt, Reaction probabilities for N_2O_5 hydrolysis on sulfate acid and ammonium sulfate aerosols at room temperature, *J. Phys. Chem. A, 101,* 871-878, 1997.

Jacob, D.J., Heterogeneous chemistry and tropospheric ozone, *Atmos. Environ., 34,* 2131-2159, 2000.

Jayne, J.T., D.R. Worsnop, C.E. Kolb, E. Schwartz, and P. Davidovits, Uptake of gas-phase formaldehyde by aqueous acid surfaces, *J. Phys. Chem., 100,* 8015-8022, 1996.

Kasibhatla, P., W.L. Chameides, and J.S. John, A three-dimensional global model investigation of seasonal variations in the atmospheric burden of anthropogenic sulfate aerosols, *J. Geophys. Res., 102,* 3737-3759, 1997.

Kiehl, J.T., and B.P. Briegleb, The relative roles of sulfate aerosols and greenhouse gases in climate forcing, *Science, 260,* 311-314, 1993.

Kleffmann, J., K.H. Becker, M. Lackhoff, and P. Wiesen, NO_2 conversion processes on carbonaceous surfaces, paper presented at Sixth Scientific Conference of the International Global Atmospheric Chemistry Project (IGAC), Bologna, Italy, Sept. 13-17, 1999.

Kolb, C.E., D.R. Worsnop, M.S. Zahniser, P. Davidovits, L.F. Keyser, M.T. Leu, M.J. Molina, D.R. Hanson, and A.R. Ravishankara, Laboratory studies in atmospheric heterogeneous chemistry, in *Progress and Problems in Atmospheric Chemistry,* edited by J.R. Baker, pp. 771-875, World Sci. River Edge, N. J., 1995.

Leaitch, R., Vertical sulfuric profiles from aircraft used in COSAM, paper presented at WCRP/IGAC Workshop, Halifax, Nova Scotia, Canada, Oct. 19-21, 1998.

Lelieveld, J., The role of clouds in tropospheric photochemistry, Ph.D. thesis, Univ. Utrecht, Utrecht, Netherlands, 1990.

Lelieveld, J., and P. Crutzen, Influences of cloud photochemical processes on tropospheric ozone, *Nature, 343,* 227-233, 1990.

Levine, S.Z., and S.E. Schwartz, In-cloud and below-cloud scavenging of acid vapor, *Atmos. Environ., 16,* 1725-1723, 1982.

Liao, H., Y.L. Yung, and J.H. Seinfeld, Effects of aerosols on the tropospheric photolysis rates in clear and cloudy atmospheres, *J. Geophys. Res., 104,* 23,697-23,707, 1999.

Liousse, C., H. Cachier, and S.G. Jennings, Optical and thermal

measurements of black carbon content in different environments: Variation of the specific attention cross-section, sigma (σ), *Atmos. Environ., 27,* 1203-1211, 1993.

Liousse, C., J.E. Penner, C. Chang, J.J. Walton, H. Eddleman, and H. Cachier, A global three- dimensional model study of carbonaceous aerosols, *J. Geophys. Res., 101,* 19,411-19,432, 1996.

Liu, S. C., et al., A study of the photochemistry and ozone budget during the Mauna Loa Observatory Photochemistry Experiment, *J. Geophys. Res., 97,* 10,463-10,471, 1992.

Longfellow, C.A., A.R. Ravishankara, and D.R. Hanson, Reactive uptake on hydrocarbon soot: Focus on NO_2, *J. Geophys. Res., 104,* 13,833-13,840, 1999.

McCormick, M.P., and T.J. Swissler, Stratospheric aerosol mass and latitudinal distribution of the El Chichón eruption for October 1982, *Geophys. Res. Lett., 10,* 877-880, 1983.

Mozurkewich, M., P. McMurry, and A. Cupta, Mass accommodation coefficient for HO_2 radicals on aqueous particles, *J. Geophys. Res., 92,* 4163-4170, 1987.

Ogren, J.A., and R.J. Charlson, Wet deposition of elemental carbon and sulfate in Sweden, *Tellus, Ser. B, 36,* 262-271, 1984.

Parungo, F., C. Nagamoto, M.Y. Zhou, A.D.A. Hansen, and J. Harris, Aeolian transport of aerosol black carbon from China to the ocean, *Atmos. Environ., 28,* 3251-3260, 1994.

Penner, J.E., H. Eddleman, and T. Novakov, Towards the development of a global inventory for black carbon emissions, *Atmos. Environ., Part A, 27,* 1277-1295, 1993.

Penner, J.E., et al., Quantifying and minimizing uncertainty of climate forcing by anthropogenic aerosols, *Bull. Am. Meteorol. Soc., 75(3),* 375-400, 1994.

Perry, R.H., and D. Green, *Perry's Chemical Engineers Handbook,* pp. 3-285, McGraw-Hill, New York, 1984.

Pitari, G., and V. Rizi, An estimate of the chemical and radiative perturbation of stratospheric ozone following the eruption of Mt. Pinatubo, *J. Atmos. Sci., 50,* 3260-3276, 1993.

Rasch, P.J., and D.L. Williamson, Sensitivity of a general circulation model climate to the moisture transport formulation, *J. Geophys. Res., 96,* 13,123-13,137, 1991.

Ravishankara, A.R., Heterogeneous and multiphase chemistry in the troposphere, *Science, 276,* 1058-1065, 1997.

Robinson, G.N., D.R. Worsnop, J.T. Jayne, C.E. Kolb, and P. Davidovits, Heterogeneous uptake of $ClONO_2$ and N_2O_5 by sulfuric acid solutions, *J. Geophys. Res., 102,* 3583-3601, 1997.

Rodriguez, J.M., M.K.W. Ko, and N.D. Sze, The role of heterogeneous conversion of N_2O_5 on sulfate aerosols in global ozone losses, *Nature, 352,* 134-137, 1991.

Rogaski, C.A., et al., Reactive uptake and hydration experiments on amorphous carbon treated with NO_2, SO_2, O_3, HNO_3, and H_2SO4, *Geophys. Res. Lett., 24,* 381-384, 1997.

Rossi, M.J., F.F. Enter, K. Tabor, F. Clothes, and L. Glitzier, Heterogeneous reactions of nitrogen oxides (NO_2, N_2O_5, HNO_3, $ClONO_2$) with surfaces representative of atmospheric aerosol, in *Heterogeneous and Liquid Phase Processes: Laboratory Studies Related to Aerosols and Clouds,* edited by P. Warneck, pp. 213-220, Springer-Verlag, New York, 1995.

Saathoff, H., S. Kamm, O. Mohler, K-H., Naumann, and U. Schurath, The interaction of soot aerosol with O_3, NO_2, NO_3, N_2O_5, HNO_3, and HO_2, paper presented at Sixth Scientific Conference of the International Global Atmospheric Chemistry Project (IGAC), Bologna, Italy, Sept. 13- 17, 1999.

Saylor, R. D., An estimate of the potential significance of heterogeneous loss to aerosols as an additional sink for hydroperoxyl radicals in the troposphere, *Atmos. Environ., 31,* 3653-3658, 1997.

Schwartz, S.E., Mass-transport considerations pertinent to aqueous phase reactions of gases in liquid water clouds, in *Chemistry of Multiphase Atmospheric System, NATO ASI Ser.*, edited by W. Jaeschke, pp. 415-472, Springer, New York, 1986.

Seinfeld, J. H., *Atmospheric Chemistry and Physics of Air Pollution,* John Wiley, New York, 1986.

Solomon, S., R. R. Garcia, F. S. Rowland, and D. J. Wuebbles, On the depletion of Antarctic ozone, *Nature, 321,* 755-758, 1986.

Tabor, K., L. Gutzwiller, and M. Rossi, The heterogeneous interaction of NO_2 with amorphous carbon, *Geophys. Res. Lett., 20,* 1431-1434, 1993.

Thlibi, J., and J.C. Petit, A study of the NOy/soot interaction in the temperature range 303-1233 K, paper presented at International Scientific Colloquium, Cologne, Germany, April 18-20, 1994.

Thomas, E.R., G.J. Frost, and Y. Rudich, Reactive uptake of ozone by proxies for organic aerosols: Surface-bound and gas-phase products, *J. Geophys. Res., 106,* 3045-3056, 2001.

Tie, X., X. Lin, and G. P. Brasseur, Two-dimensional coupled dynamical/chemical/ microphysical simulation of global distribution of El Chichon volcanic aerosols, *J. Geophys. Res., 99,* 16,779-16,792, 1994a.

Tie, X., G. P. Brasseur, B. Briegleb, and C. Granier, Two-dimensional simulation of Pinatubo aerosol and its effect on stratospheric ozone, *J. Geophys. Res., 99,* 20,545-20,562, 1994b.

Tie, X., G. P. Brasseur, C. Granier, A. De Rudder, and N. Larsen, Model study of polar stratospheric clouds and their effects on stratospheric ozone, Part I, Model results, *J. Geophys. Res., 101,* 12,575-12,584, 1996.

Turco, R.P., P. Hamill, O.B. Toon, R.C. Witten, and C.S. Kiang, A one-dimensional model describing aerosol formation and evolution in the stratosphere, I, Physical processes and numerical analogs, *J. Atmos. Sci., 36,* 699-717, 1979.

Van Doren, J.M., L.R. Watson, P. Davidovits, D.R. Worsnop, M.S. Zahniser, and C.E. Kolb, Uptake on N_2O_5 and HNO_3 by aqueous sulfuric acid droplets, *J. Phys. Chem., 95,* 1684- 1689, 1991.

Visconti, G.M., Verdecchia, and G. Pitari, A comparison of lidar data and two-dimensional simulation of dust transport from the eruption of El Chichón, *J. Atmos. Sci., 45,* 1097-1109, 1988.

Ward, D. E., W.M. Hao, R.E. Babbitt, R.W. Shea, J.B. Kauffman, C.O. Justice, Effect of fuel composition on combustion efficiency and emission factors for African savanna ecosystems, *J. Geophys. Res., 101,* 23,569-23,576, 1996.

Wesely, M.L.,and B.B. Hicks, A review of the current status of knowledge on dry deposition, *Atmos. Environ., 34,* 2261-2282, 2000.

Zhang, R.Y., M.T. Leu, and L.F. Keyser, Sulfuric acid monohydrate: Formation and heterogeneous chemistry in the stratosphere, *J. Geophys. Res., 100,* 18,845-18.854, 1995.

G. Brasseur, Max-Planck-Institute of Meteorology, 20146 Hamburg, Germany.

L. Emmons, D. Kinnison, and X. Tie, National Center for Atmospheric Research, Boulder, CO 80303.

L. Horowitz, Princeton University, Princeton, NJ 08542-0308.

(Received September 12, 2000; revised March 23, 2001; accepted April 24, 2001.)